Progress in the radiative modeling of ice clouds and dust aerosols for MODIS-based remote sensing

Ping Yang[1,2] and George Kattawar[2]

1. Department of Atmospheric Sciences

2. Department of Physics &Astronomy

Texas A&M University, College Station, TX 77843

In collaboration with

Andrew Dessler, Gerald North

Bryan Baum, Andrew Heymsfield, Yongxiang Hu

Steven Platnick, Michael King, Bo-Cai Gao, Zhibo Zhang

Si-Chee Tsay, Christina N. Hsu, Istvan Laszlo and Ralph Kahn

with contributions by

L. Bi, H.-M. Cho, S. Ding, Q. Feng, G. Hong, Y .Li, K. Meyer, Y. Xie, Y. You

TEXAS A&M UNIVERSITY

The MODIS cloud property products provide an unprecedented opportunity to

- **develop the climatologies of cloud microphysical and optical properties from a global perspective**
- **assess the performance of climate models**

- Data: GSFC-MODIS and LaRC-MODIS Aqua level 3 (1º×1º) daytime only cloud property products

- Range: July 2002 to June 2007, 60ºN to 60ºS

-CAM3: T42 (128 by 64), 26 vertical levels

- Use observed monthly mean sea surface temperature and sea ice concentration (Hurrell et al., 2008) to force the climate model

Geographical Distribution of Cloud Fraction

Terra **Aqua**

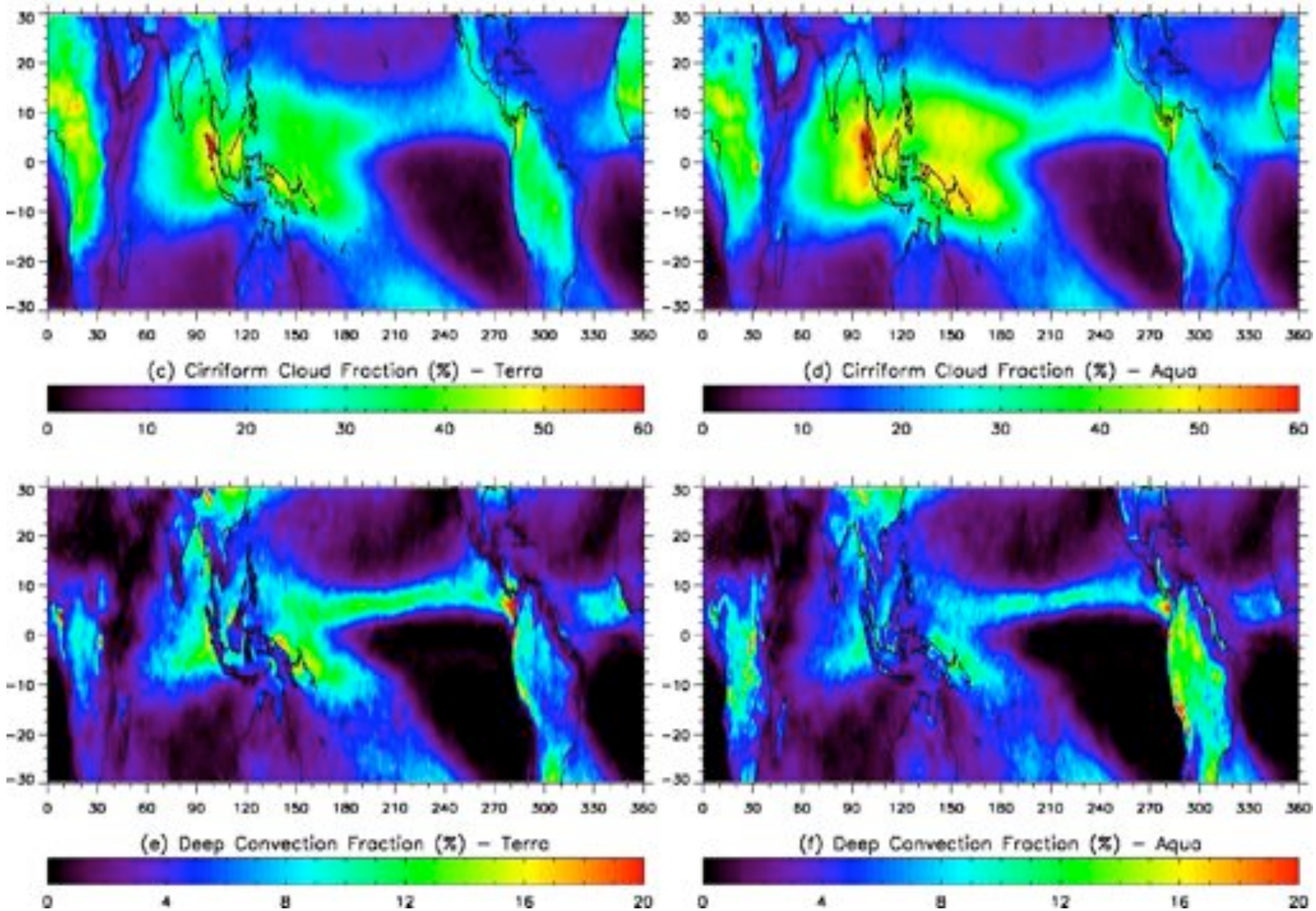

Hong, Yang and co-authors (2007)

Geographical Distribution of Cloud Properties

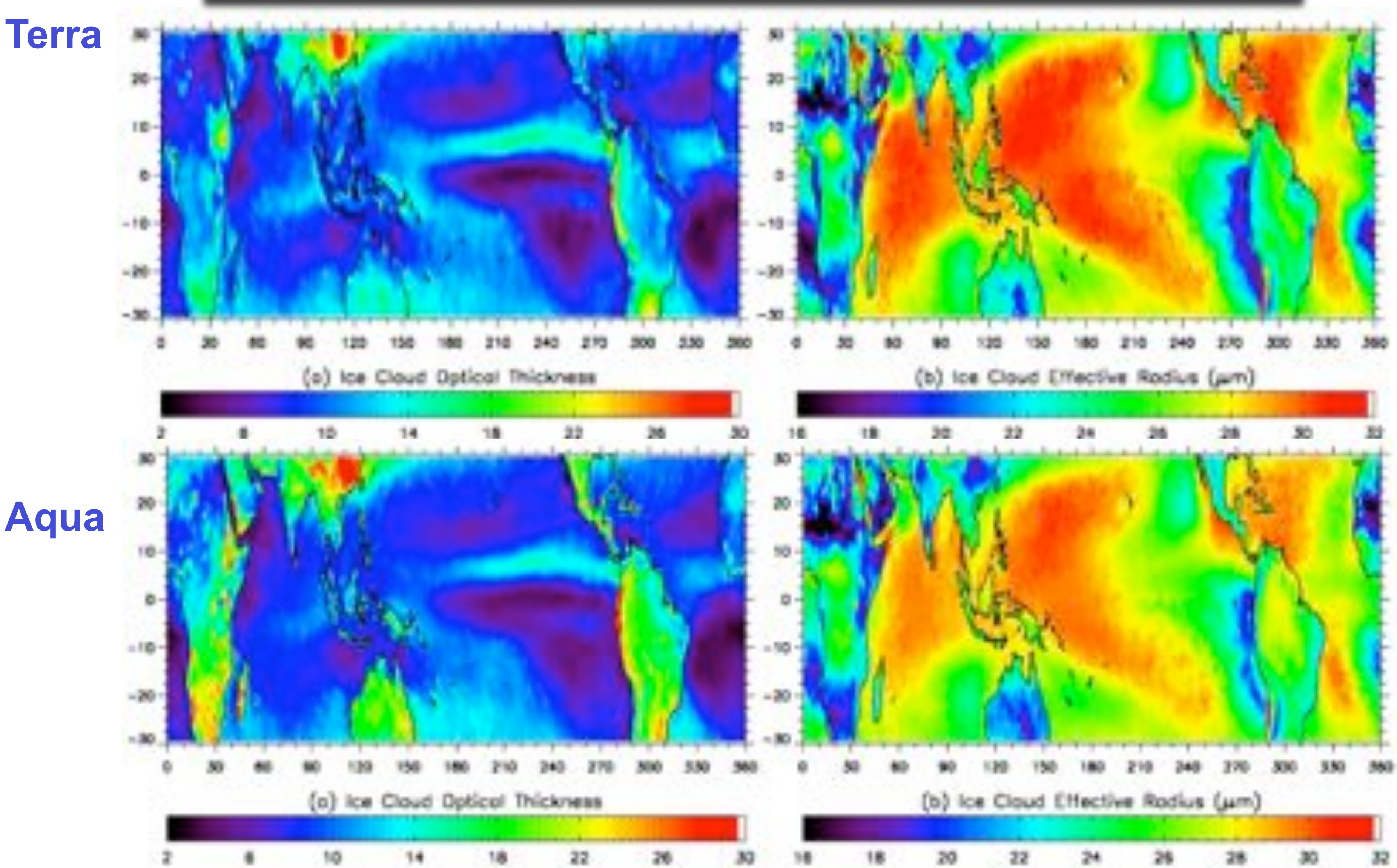

Hong, Yang and co-authors (2007)

Total Cloud Fraction (%)

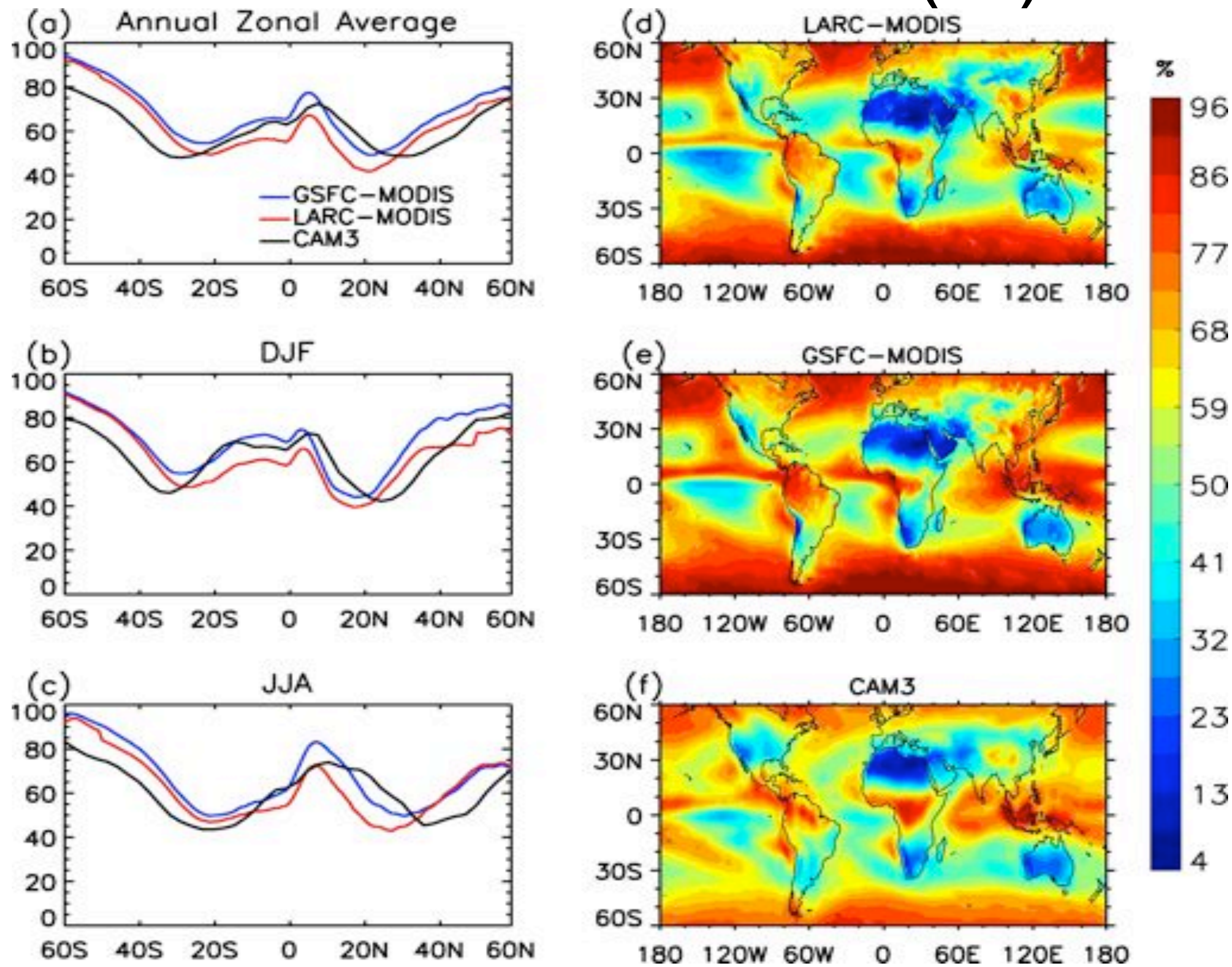

Left column: Zonal distribution of cloud fraction from GSFC-MODIS, LaRC-MODIS and CAM3. Annual average (a), DJF (b) and JJA (c) seasons are plotted separately. Right column: Annual mean cloud fraction distributions from LaRC-MODIS (d), GSFC-MODIS (e) and CAM3 (f).

Cloud Liquid Water Path (gm^{-2})

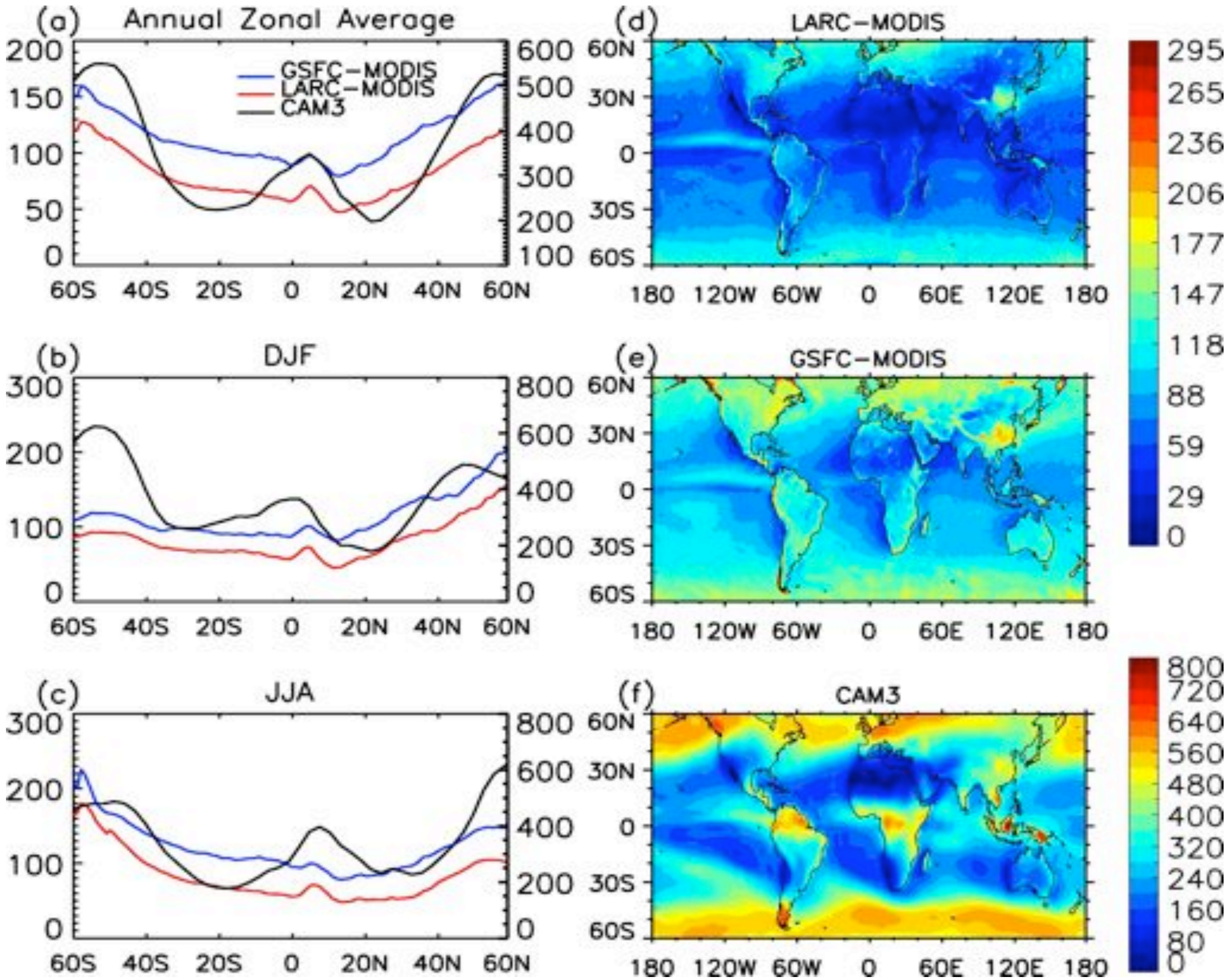

Cloud Ice Water Path (gm^{-2})

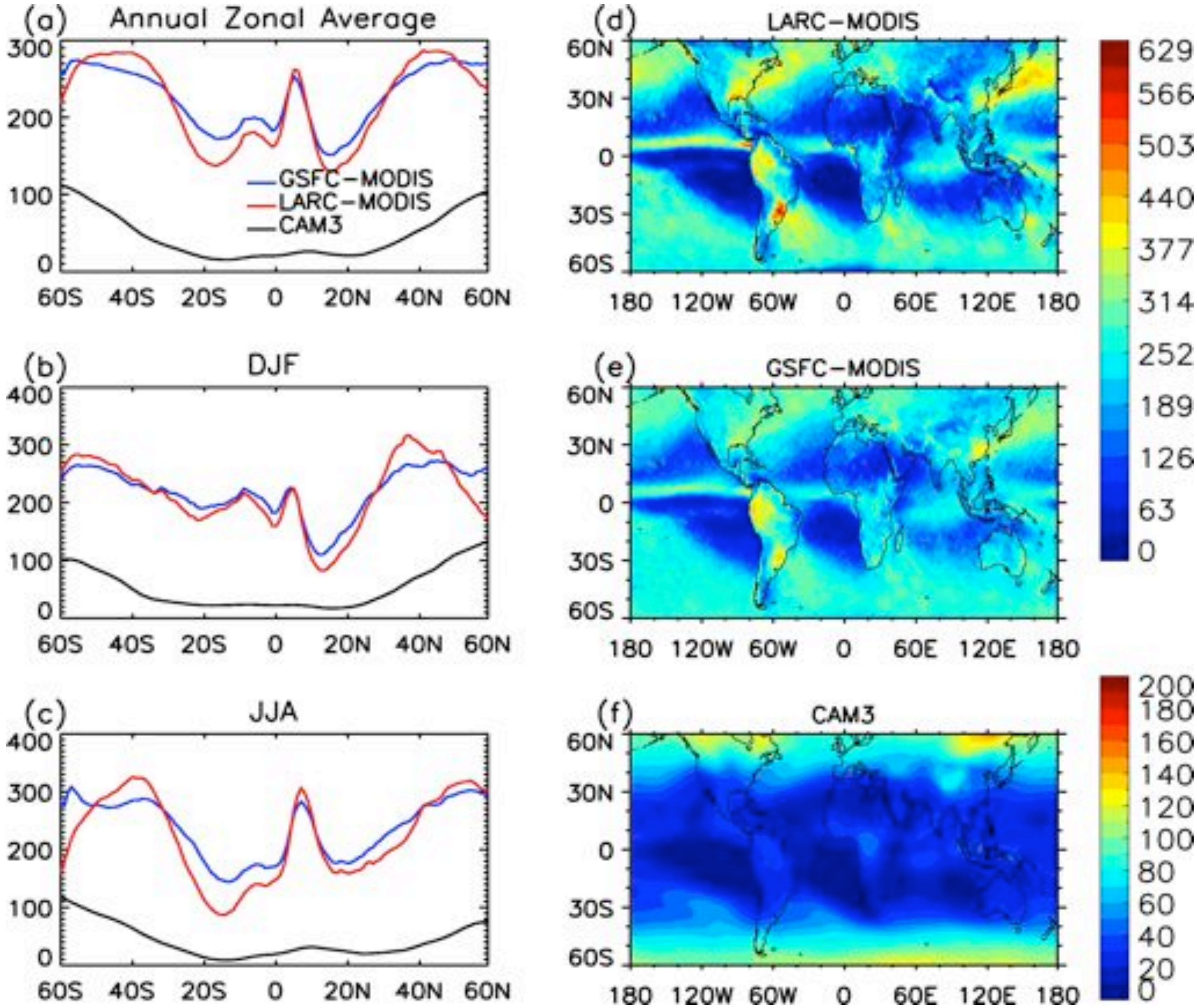

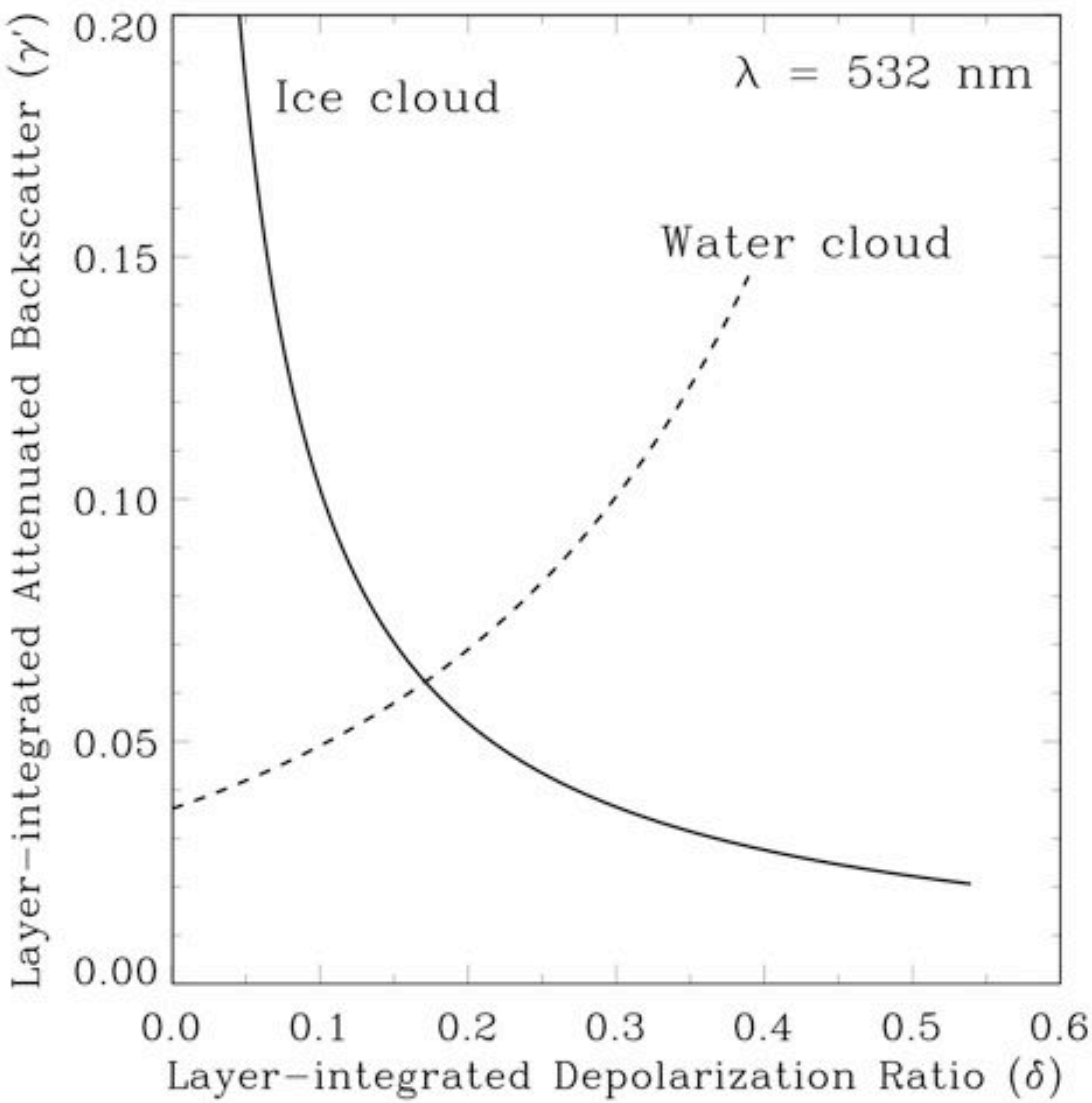

Fig. 1. Schematic curves showing the relationships (Hu et al. [8]) between the layer-integrated depolarization ratio and layer-integrated attenuated backscatter coefficient for ice clouds (solid line) and water clouds (dashed line).

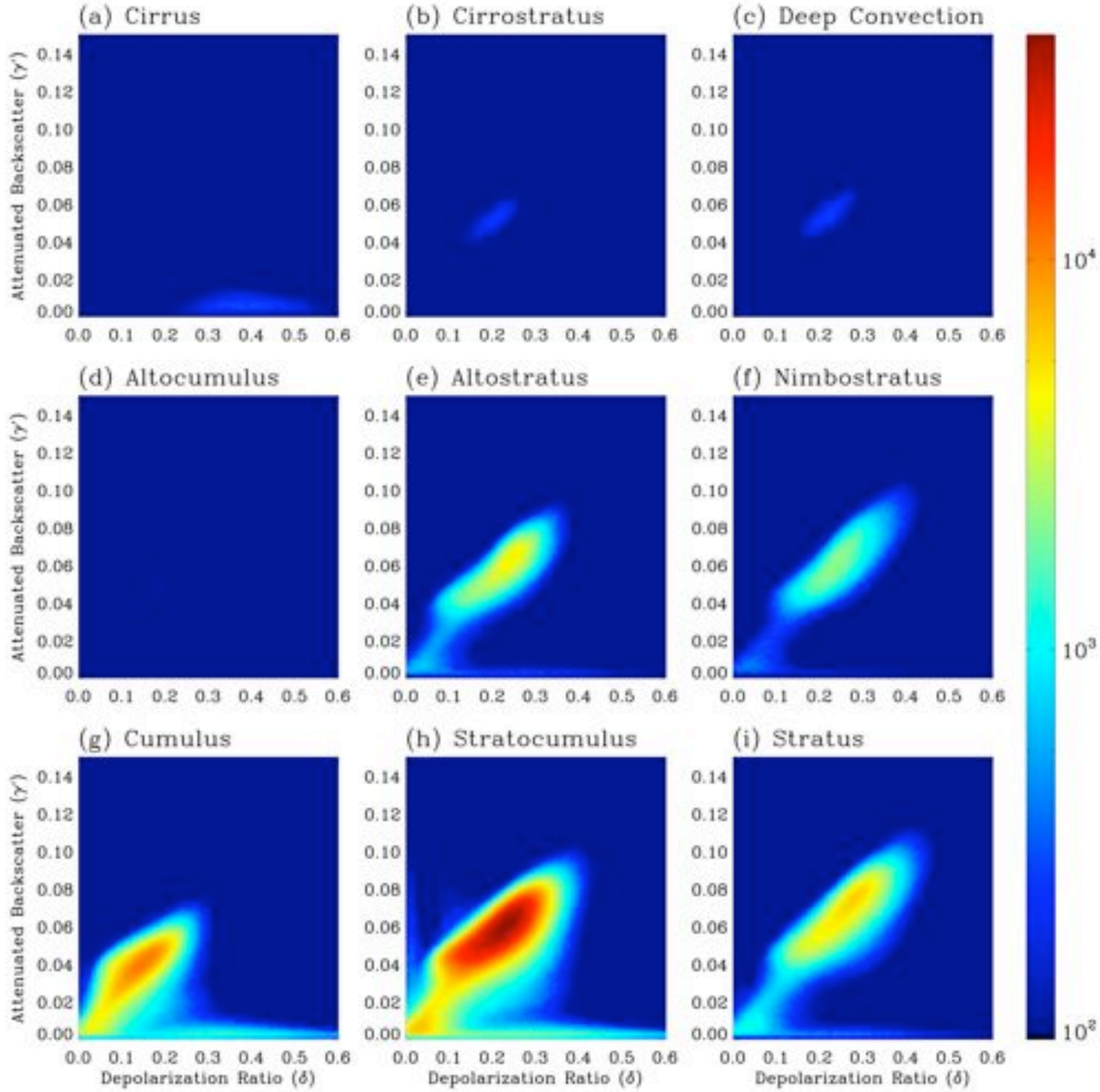

The $\delta - \gamma'$ relationships for the clouds flagged as in water-phase by the MODIS IR cloud-phase determination algorithm .

Liquid Particle Effective Radius (μm)

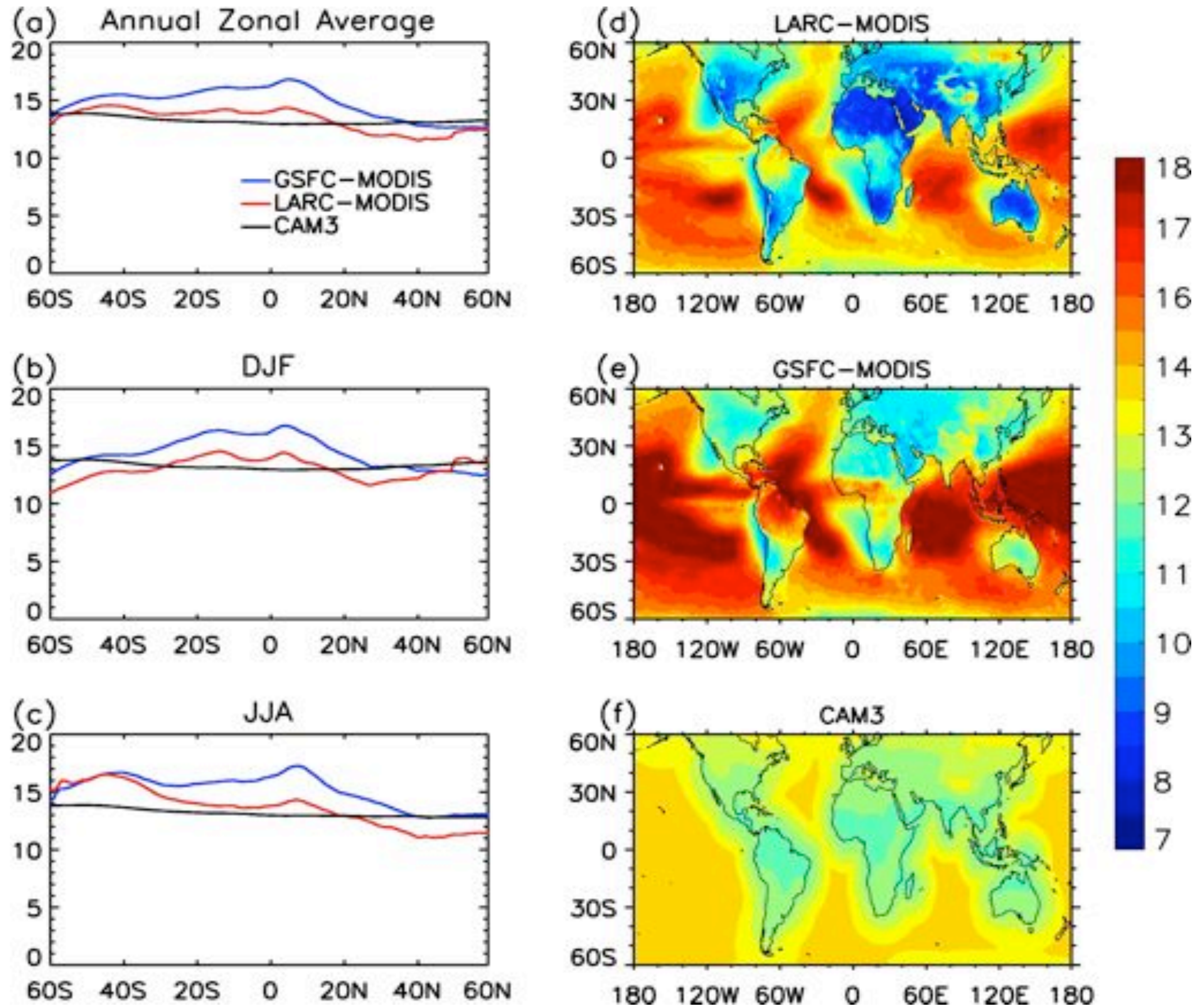

Ice Particle Effective Radius (μm)

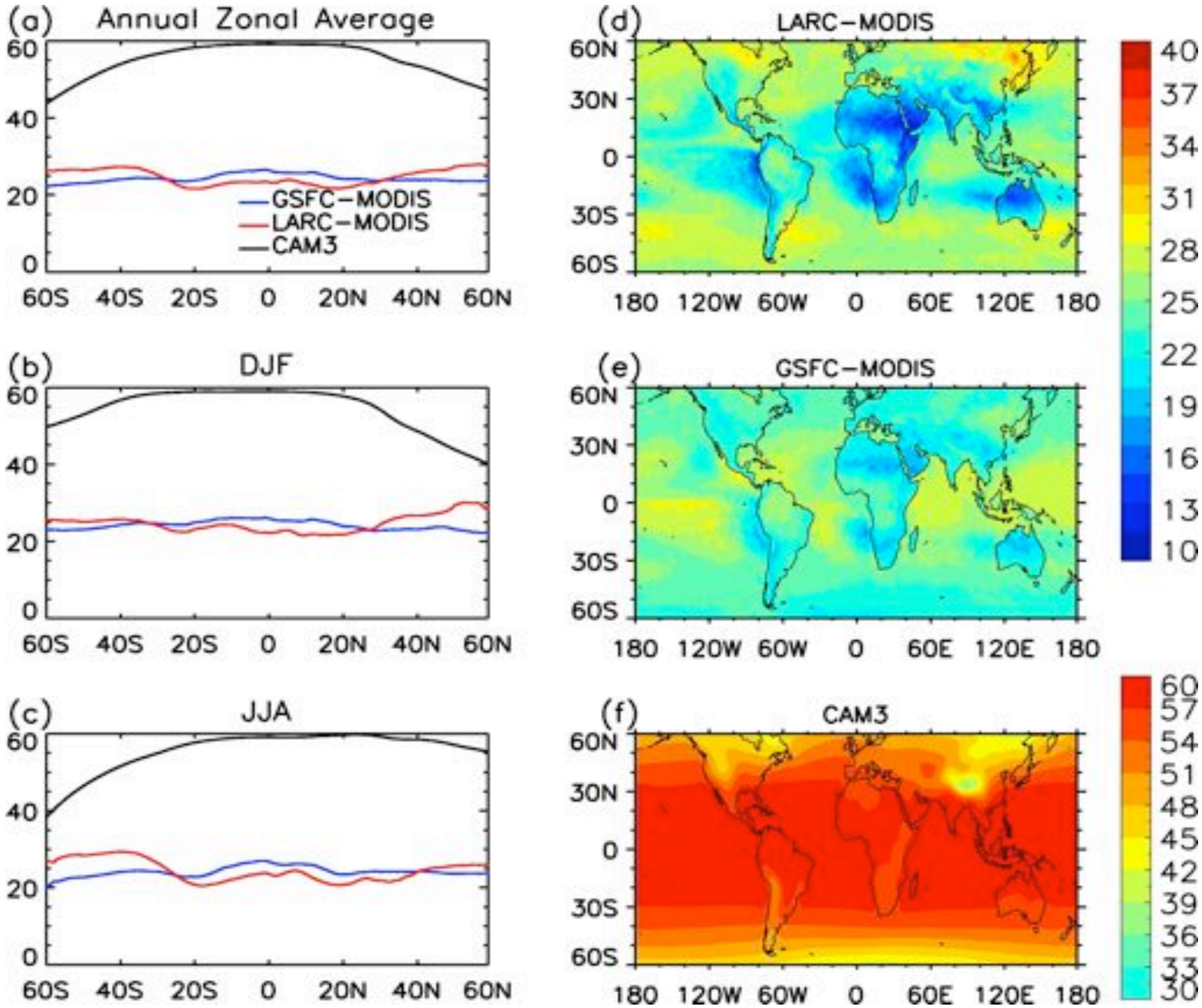

Water Cloud Optical Depth

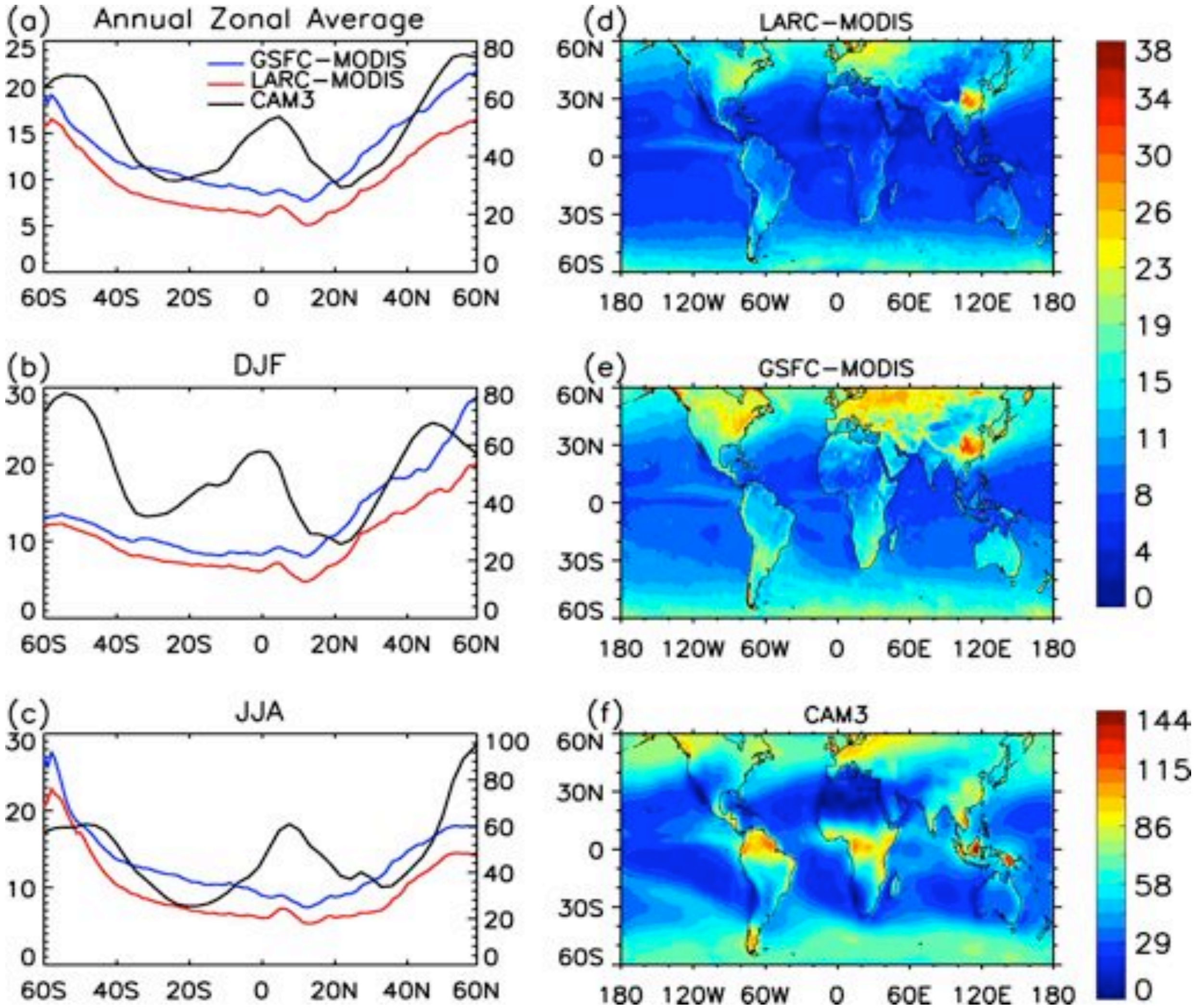

Ice Cloud Optical Depth

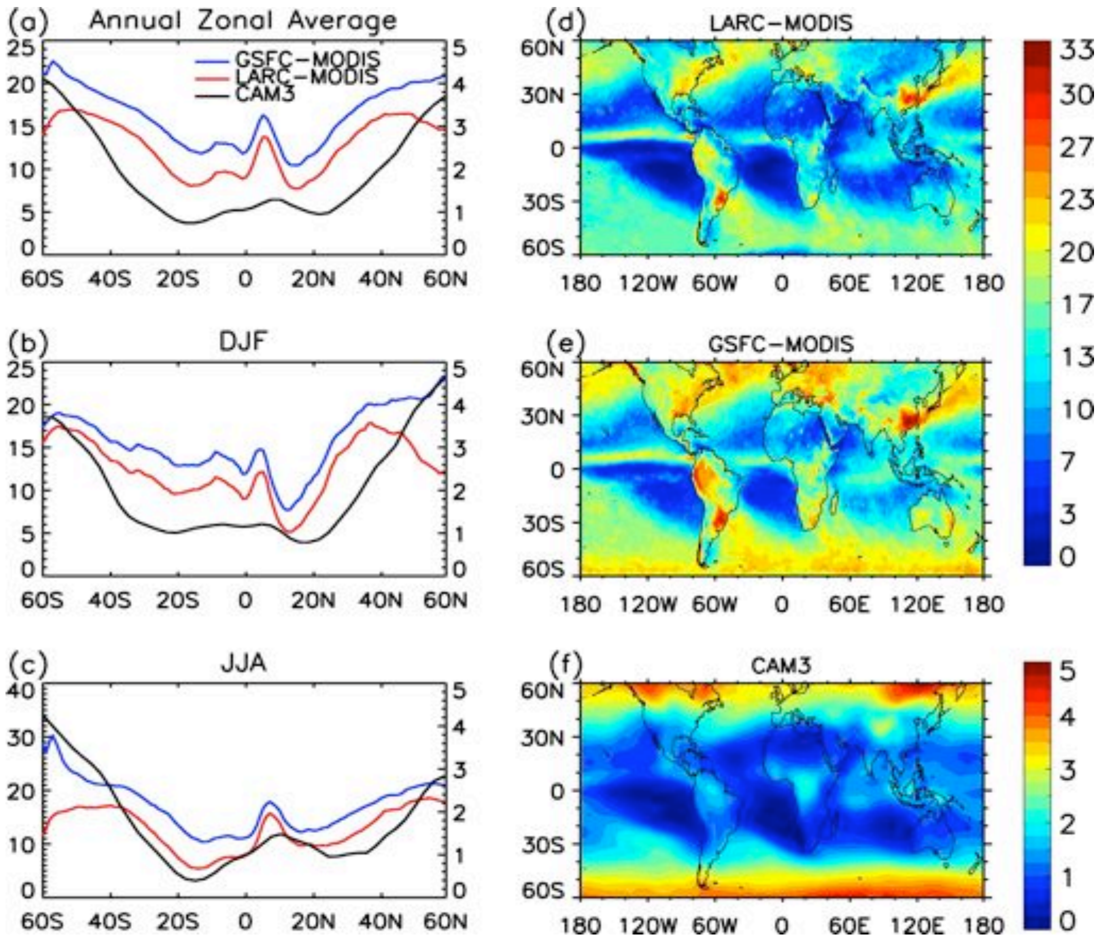

Equatorial Wave Spectrum

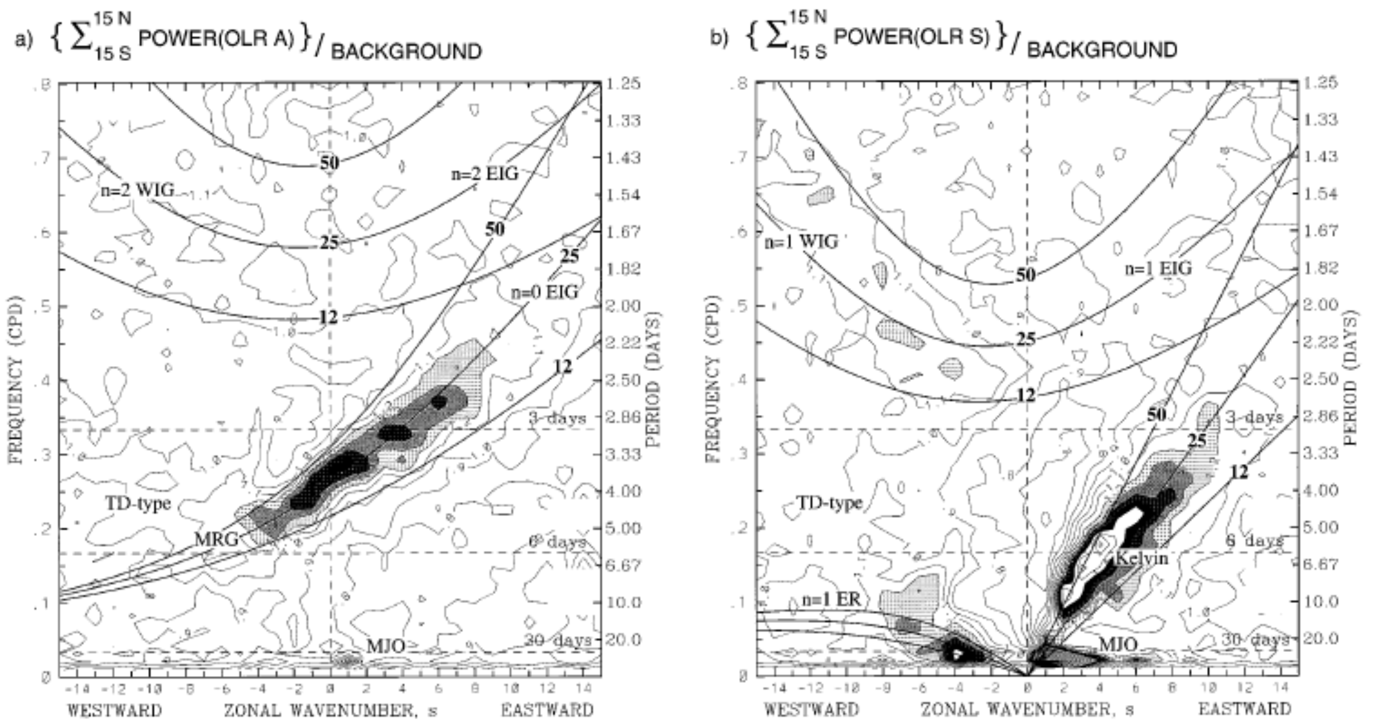

FIG. 3. (a) The antisymmetric OLR power of Fig. 1a divided by the background power of Fig. 2. Contour interval is 0.1, and shading begins at a value of 1.1 for which the spectral signatures are statistically significantly above the background at the 95% level (based on 500 dof). Superimposed are the dispersion curves of the even meridional mode-numbered equatorial waves for the three equivalent depths of h = 12, 25, and 50 m. (b) Same as in panel a except for the symmetric component of OLR of Fig. 1b and the corresponding odd meridional mode-numbered equatorial waves. Frequency spectral bandwidth is 1/96 cpd.

Wheeler and Kiladis,1999

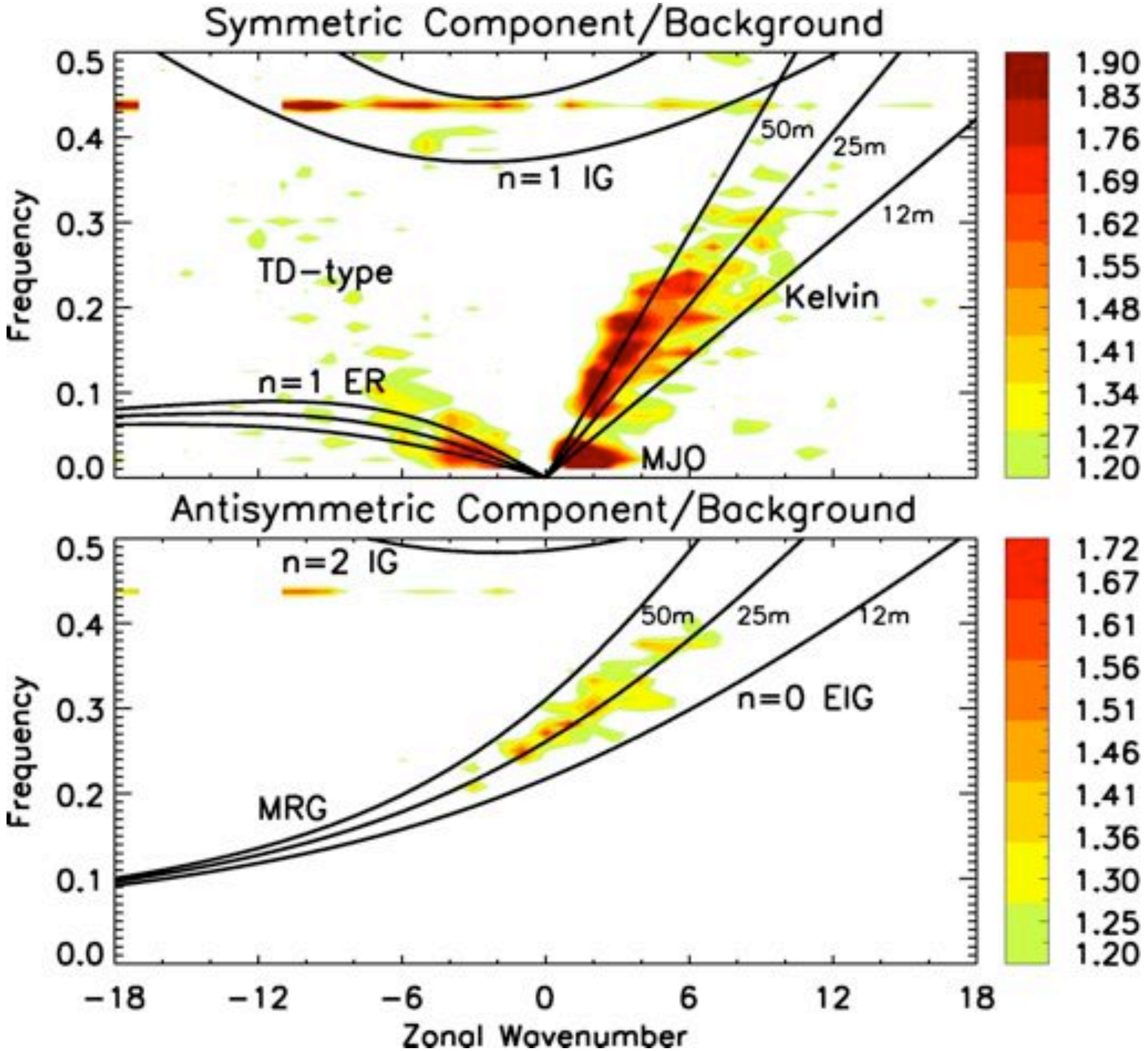

Symmetric Component/Background
n=1 IG
50m
25m
12m
TD-type
Kelvin
n=1 ER
MJO
Frequency
1.90
1.83
1.76
1.69
1.62
1.55
1.48
1.41
1.34
1.27
1.20
Antisymmetric Component/Background
n=2 IG
50m
25m
12m
n=0 EIG
MRG
Frequency
1.72
1.67
1.61
1.56
1.51
1.46
1.41
1.36
1.30
1.25
1.20
Zonal Wavenumber

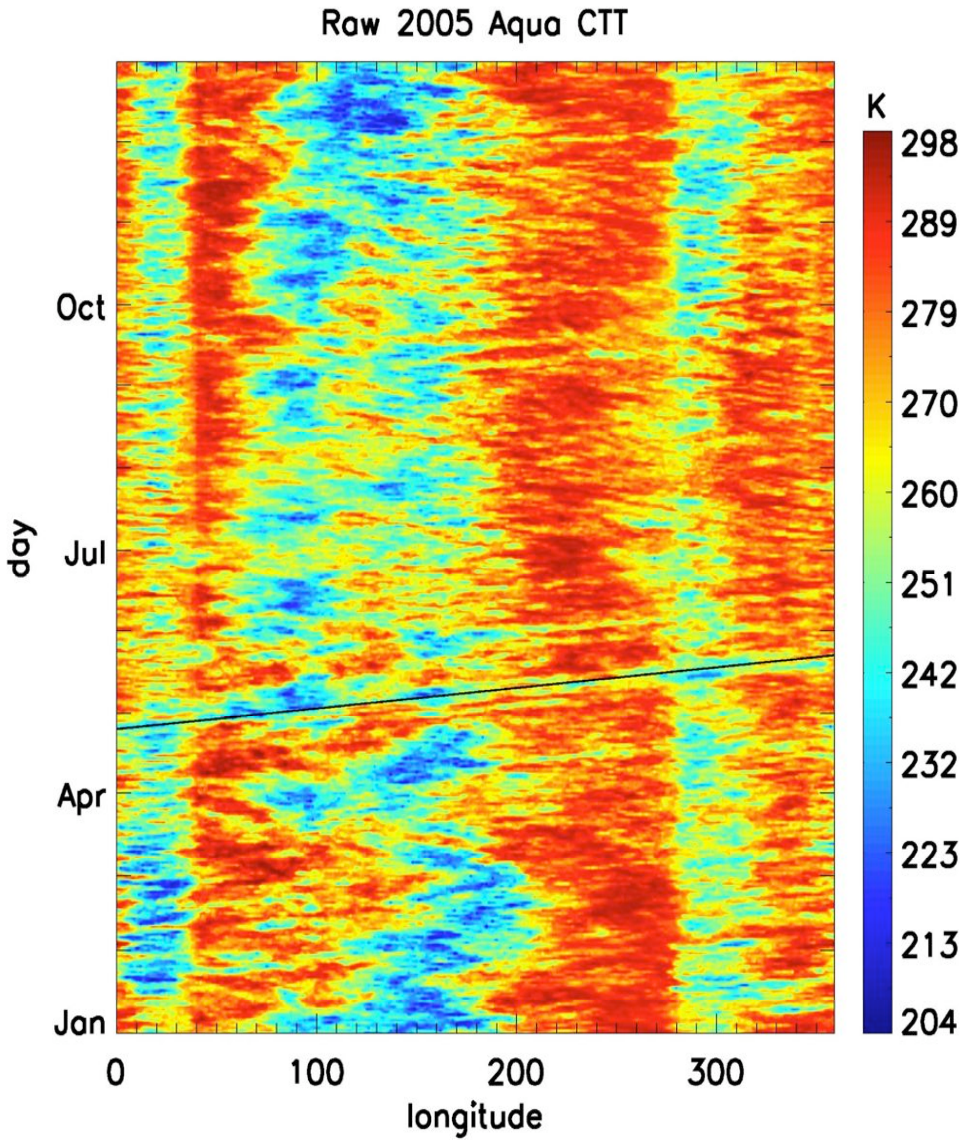

Left panel: Hovmöller Diagram of raw CTT averaged between 15°N and 15°S of year 2005 from MODIS Aqua data. The thick line corresponds to phase speed of 15 ms^{-1}

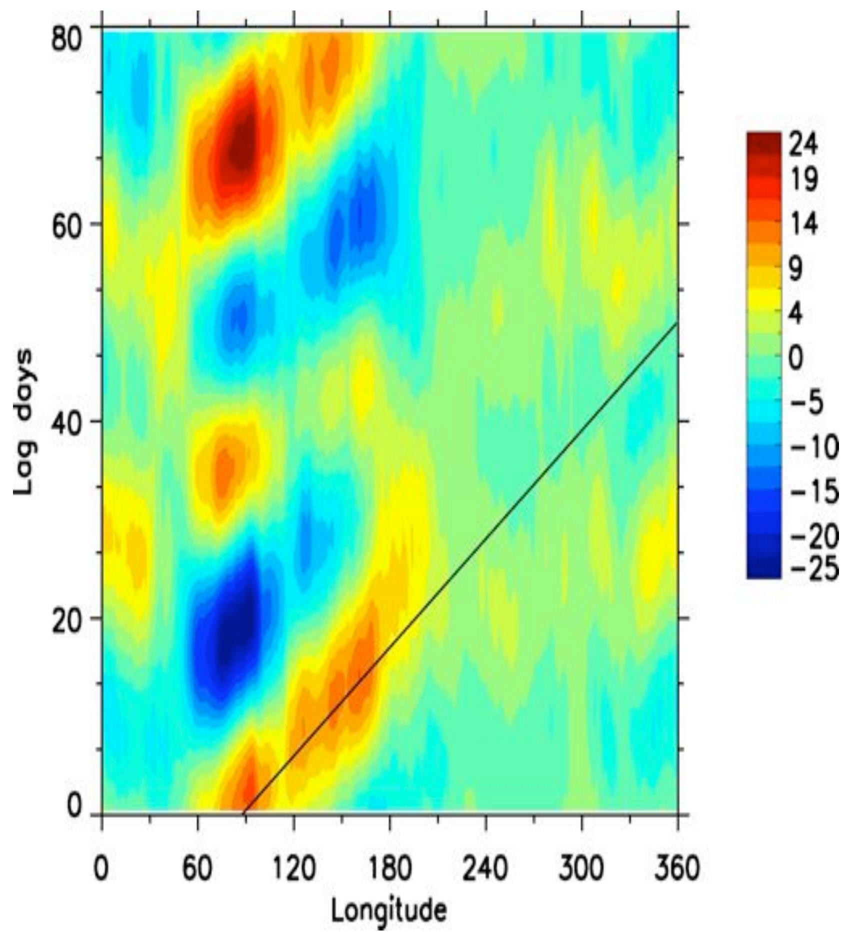

Right panel: Longitude-lagday cross section of EEOF 5 of CTT averaged between 5°N and 5°S. Units are arbitrary.
The thick line indicates a phase speed of 7 ms^{-1}

Light scattering and radiative transfer simulations are fundamental to the retrieval of cloud and aerosol properties from MODIS measurements

Scattering Geometry

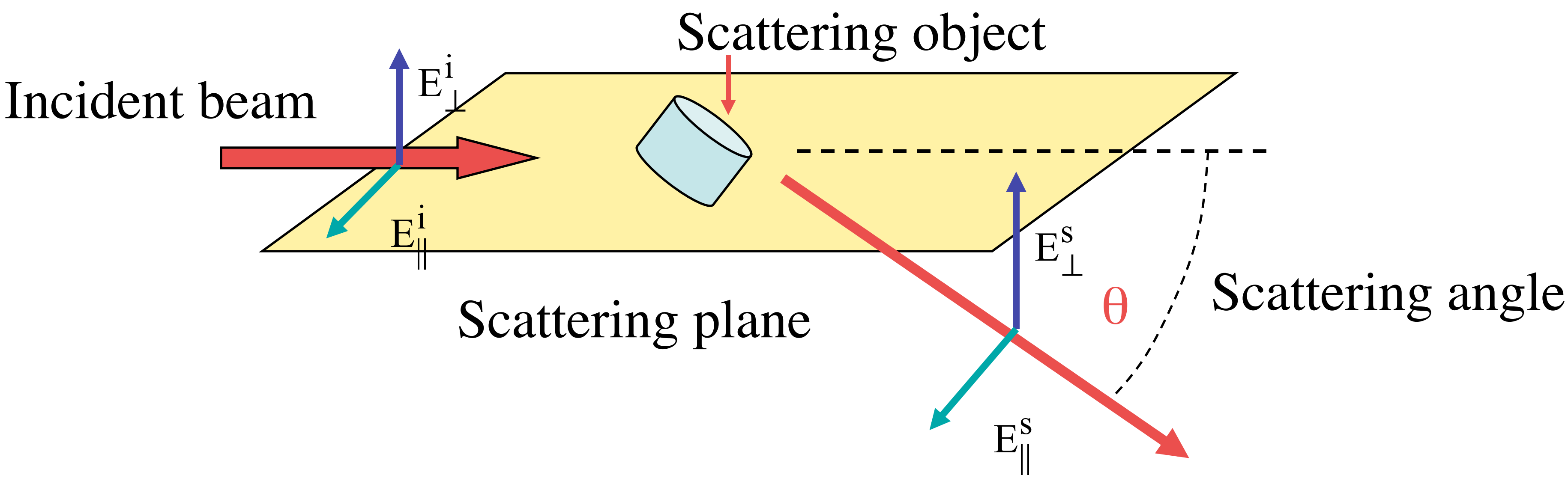

Amplitude scattering matrix

$$\begin{pmatrix} E^s_\parallel \\ E^s_\perp \end{pmatrix} = \frac{e^{ikr}}{-ikr} \begin{pmatrix} S_2 & S_3 \\ S_4 & S_1 \end{pmatrix} \begin{pmatrix} E^i_\parallel \\ E^i_\perp \end{pmatrix}$$

Stokes vector-Phase matrix/Mueller matrix formulation

The electric field can be resolved into components. $E_{//}$ and $E_{\perp}$ are complex oscillatory functions.

$$\mathbf{E} = E_{//}\,\mathbf{l} + E_{\perp}\,\mathbf{r}$$

The four component Stokes vector (Stokes, 1852) can now be defined, which are all real numbers.

$$I = E_{//}E_{//}^{*} + E_{\perp}E_{\perp}^{*}$$

$$Q = E_{//}E_{//}^{*} - E_{\perp}E_{\perp}^{*}$$

$$U = E_{//}E_{\perp}^{*} + E_{\perp}E_{//}^{*}$$

$$V = i(E_{//}E_{\perp}^{*} - E_{\perp}E_{//}^{*})$$

Ellipticity= Ratio of semiminor to semimajor axis of polarization ellipse=b/a

$=\tan[(\sin^{-1}(V/I))/2]$

Nissan car viewed in mid-wave infrared

I

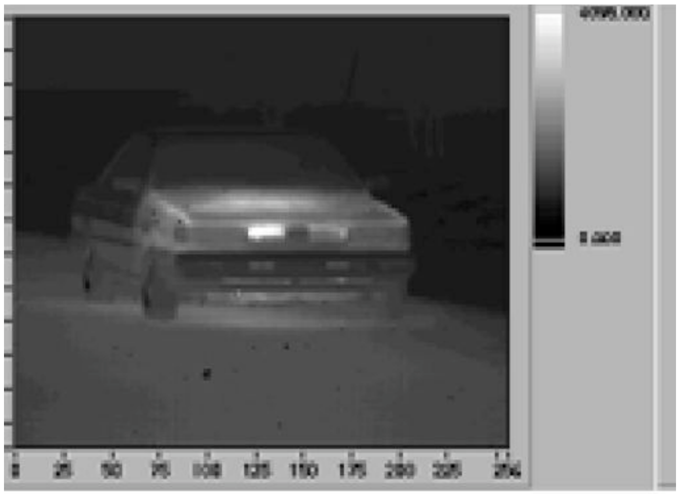

Ellipticity

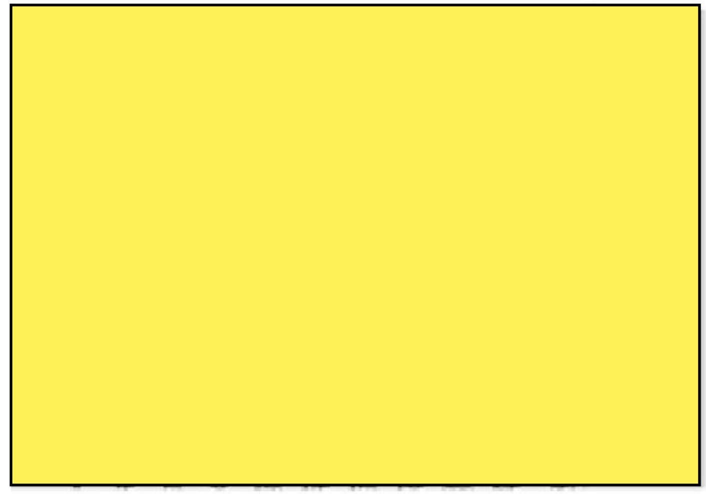

This data was collected using an Amber MWIR InSb imaging array 256x256. The polarization optics consisted of a rotating quarter wave plate and a linear polarizer. Images were taken at eight different positions of the quarter wave plate (22.5 degree increments) over 180 degrees. The data was reduced to the full Stokes vector using a Fourier transform data reduction technique. Courtesy of Brume Blume, Nicoholls Co.

Phase matrix

The phase matrix, P, relates the incident and scattered Stokes vectors. The first element of the phase matrix is called the phase function that describes the angular distribution of scattered energy.

For an ensemble of cloud particles with their mirror positions in equal number and in random orientation, the mean phase matrix has six independent elements.

$$\begin{pmatrix} I_s \\ Q_s \\ U_s \\ V_s \end{pmatrix} = \frac{\sigma_s}{4\pi k^2 r^2} \begin{pmatrix} P_{11} & P_{12} & 0 & 0 \\ P_{12} & P_{22} & 0 & 0 \\ 0 & 0 & P_{33} & P_{34} \\ 0 & 0 & -P_{34} & P_{44} \end{pmatrix} \begin{pmatrix} I_i \\ Q_i \\ U_i \\ V_i \end{pmatrix}$$

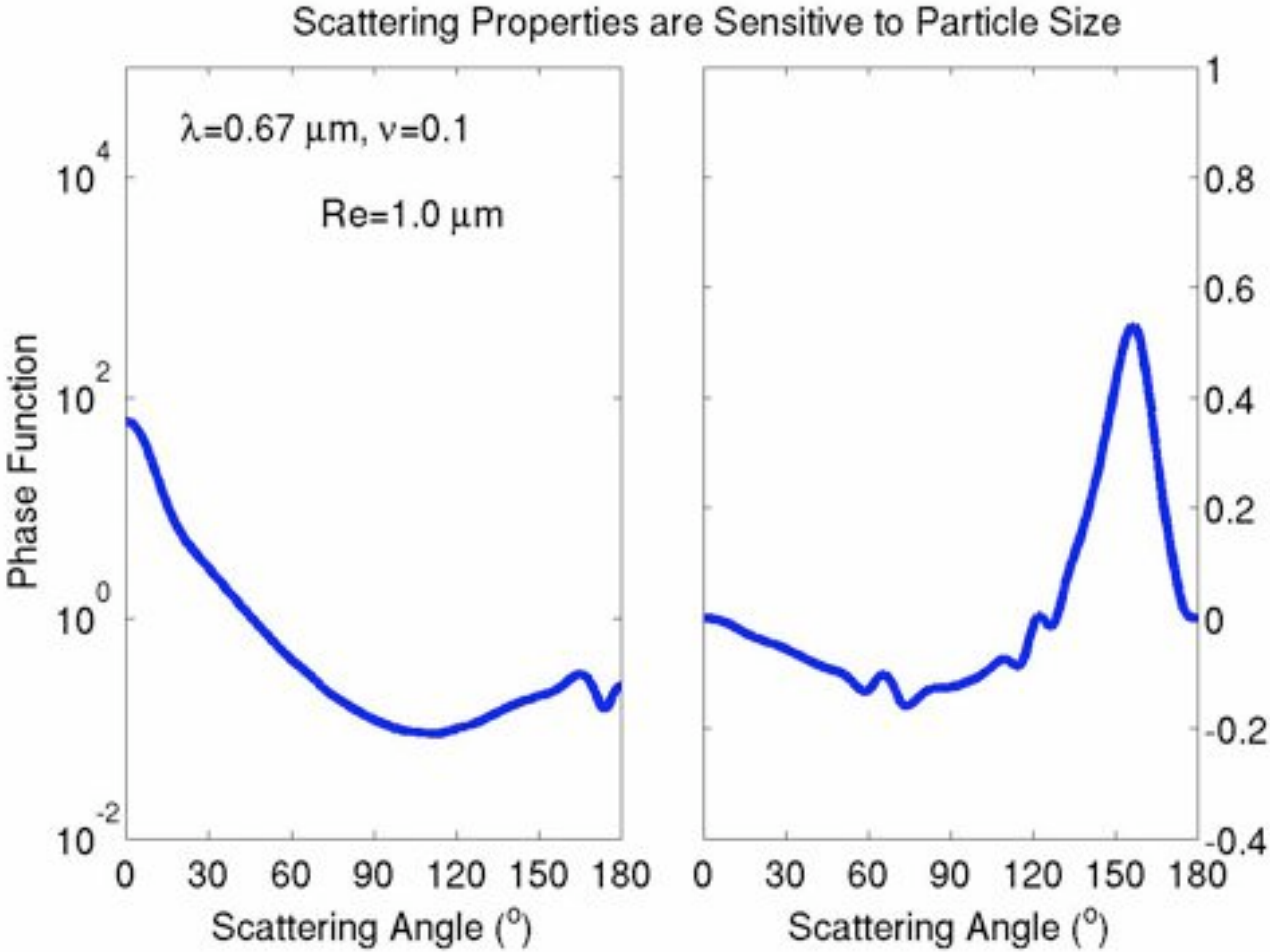

Scattering Properties are Sensitive to Particle Size
λ=0.67 μm, ν=0.1
Re=1.0 μm
Phase Function
10^4
10^2
10^0
10^-2
0 30 60 90 120 150 180
Scattering Angle (°)
-P12/P11
1
0.8
0.6
0.4
0.2
0
-0.2
-0.4
0 30 60 90 120 150 180
Scattering Angle (°)

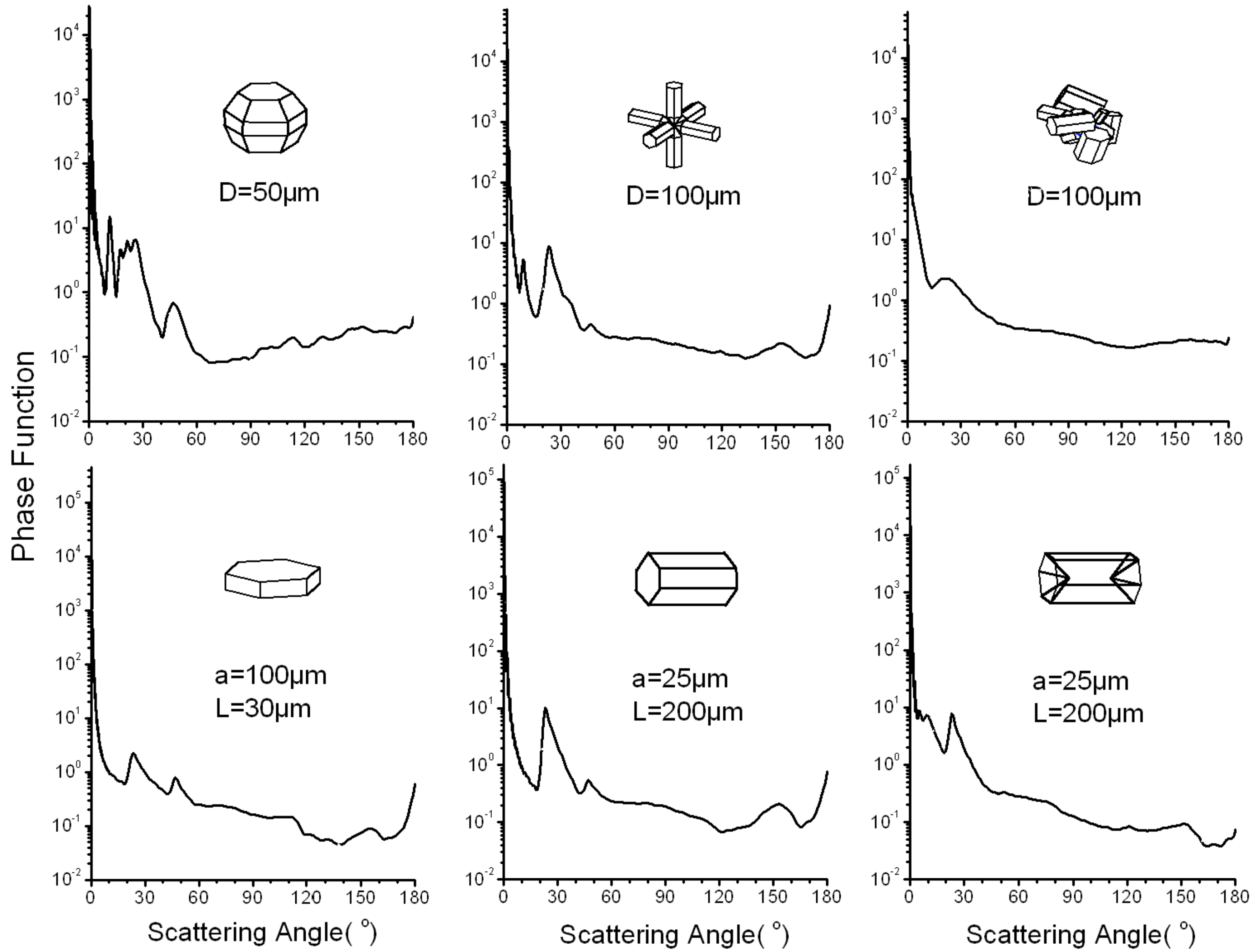

Yang, P. and K. N. Liou, 2006: Light Scattering and Absorption by Nonspherical Ice Crystals, in ***Light Scattering Reviews: Single and Multiple Light Scattering,*** Ed. A. Kokhanovsky, Springer-Praxis Publishing, Chichester, UK, 31-71.

Simultaneous retrieval of cloud optical thickness and effective particle size (the Nakajima-King algorithm)

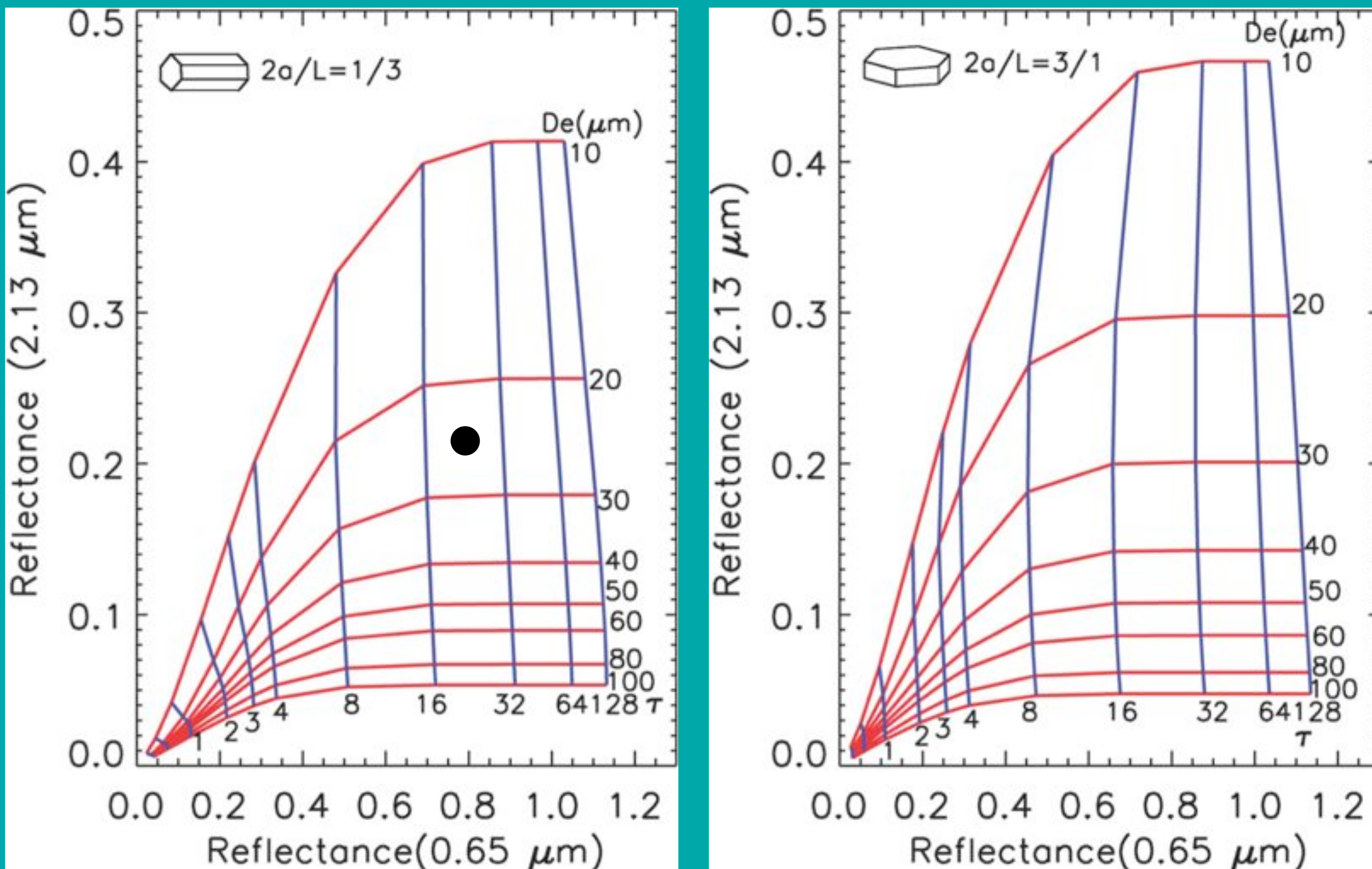

Finite-difference time domain (FDTD) simulation process

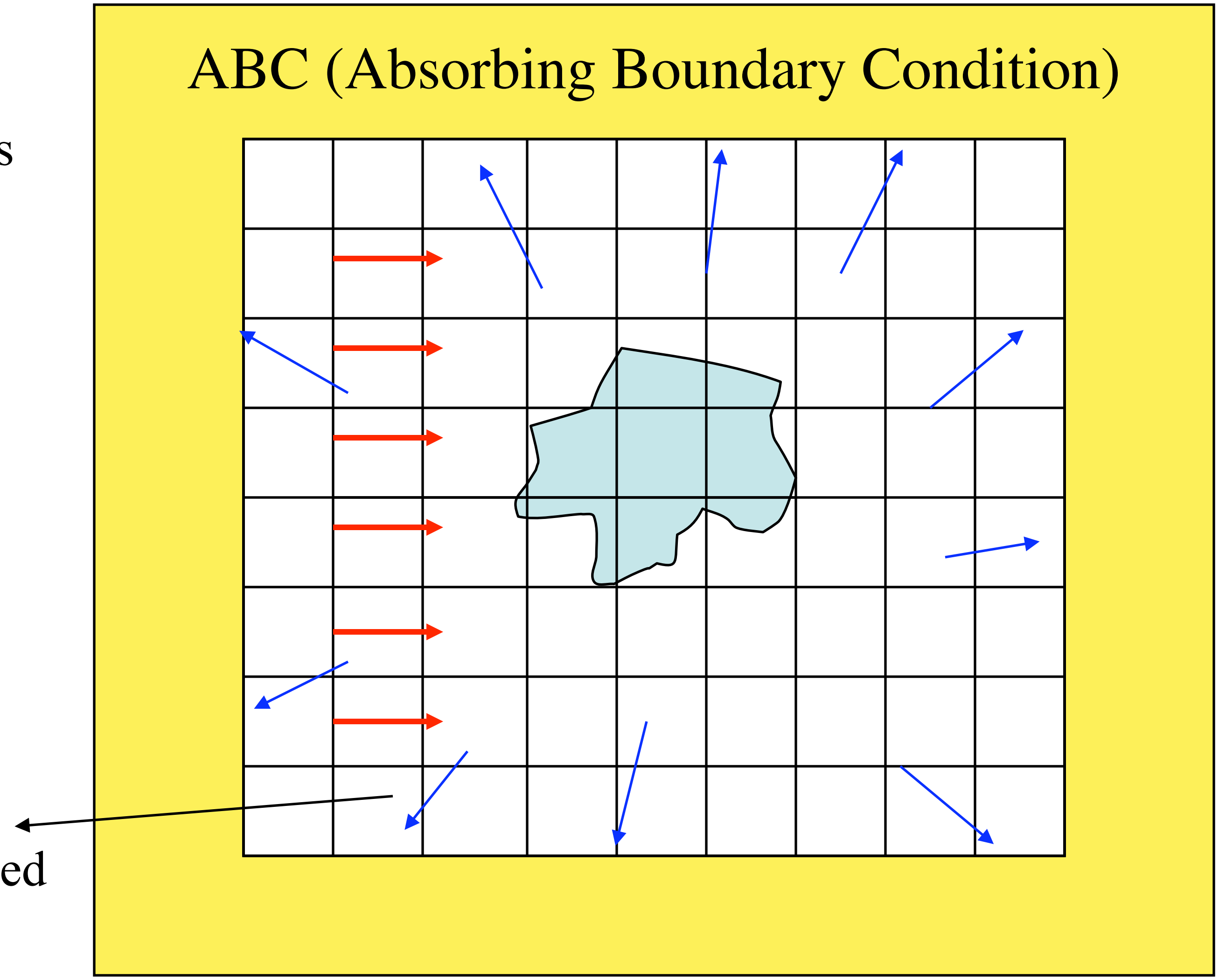

Plane parallel Incident light is applied on a surface which encloses the particle

only scattered fields

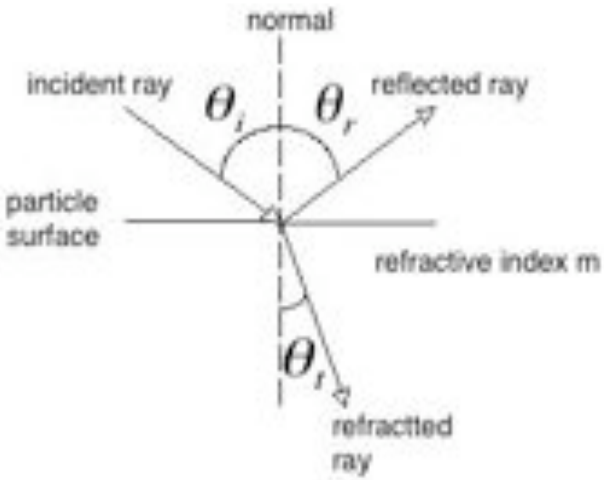

Snell's Law

$$\theta_i = \theta_r$$

$$\frac{\sin\theta_i}{\sin\theta_t} = m$$

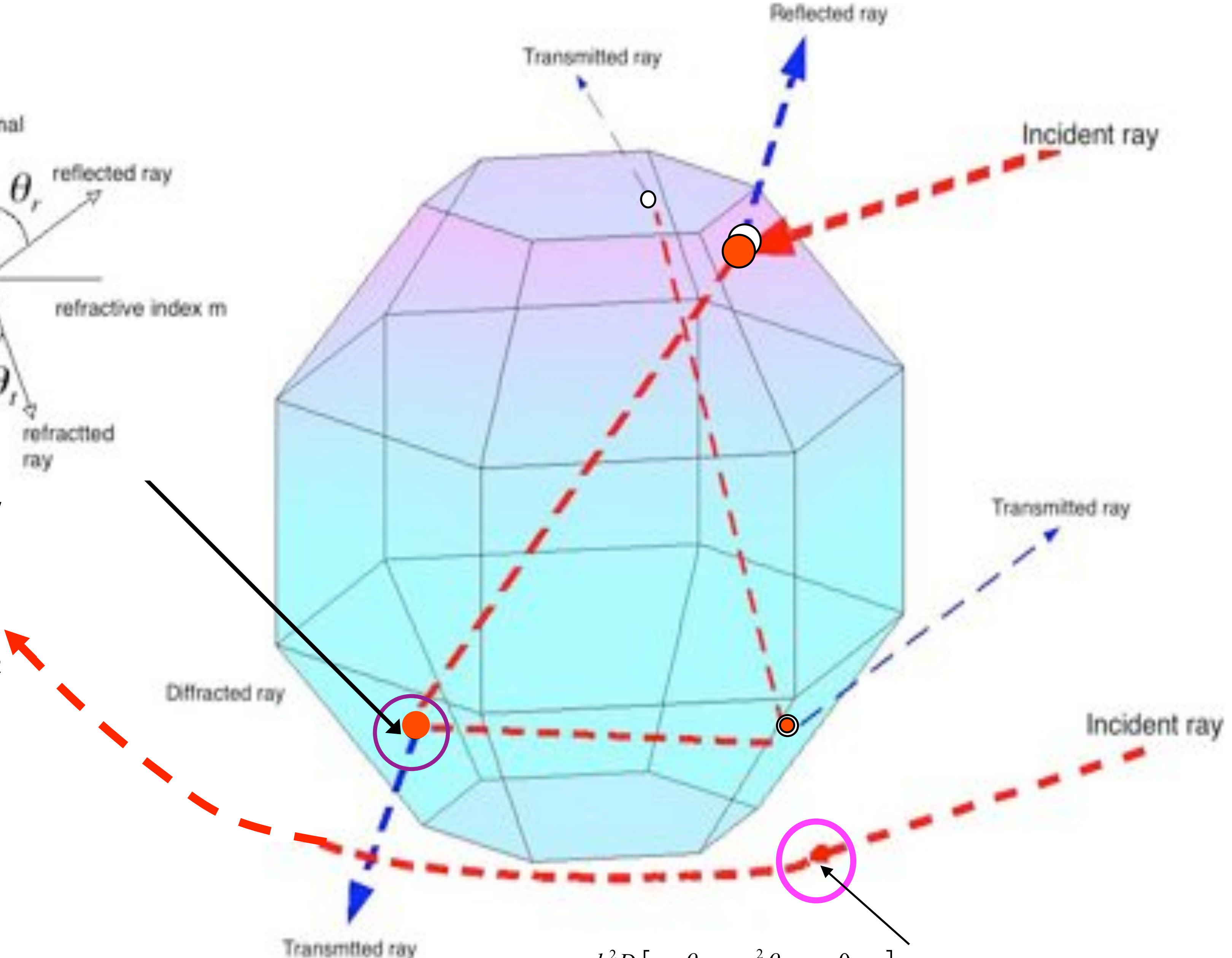

$$S_d = \frac{k^2 D}{4\pi}\begin{bmatrix}\cos\theta + \cos^2\theta & 0 \\ 0 & 1+\cos\theta\end{bmatrix} \qquad D = \iint_P \exp(ik\hat{r}_s \cdot \vec{\xi})\, d^2\xi$$

Ice cloud models: MODIS Collection 004 vs 005

Mixing schemes for ice cloud particles MODIS Collection 4 *(King et al., 2004)*

Particle's maximum dimension D < 70 μm

 50% + 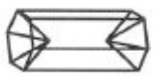 25% +  25%

70 μm < D

 30% +  30% +

 20% +  20%

Mixing schemes for ice cloud particles MODIS Collection 5 *(Baum et al. 2005; King et al., 2007)*

Particle's maximum dimension D < 60 μm

 100%

60 μm < D < 1000 μm

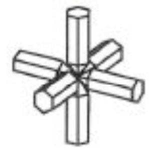 15% + 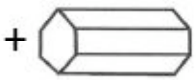 50% +  35%

1000 μm < D < 2500 μm

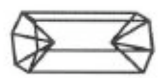 45% + 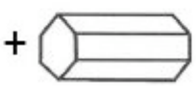 45% +  10%

2500 μm < D

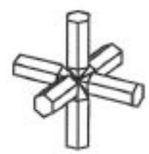 97% + 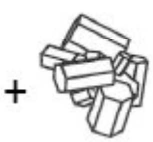 3%

New habit: Droxtal

Courtesy of Andy Heymsfield

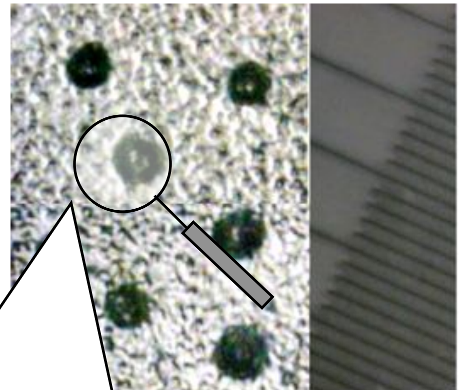

- Predominant in the uppermost portions of cirrus clouds
- 20-Faced Polyhedron
  - 12 isosceles trapezoid
  - 6 rectangular
  - 2 hexagonal

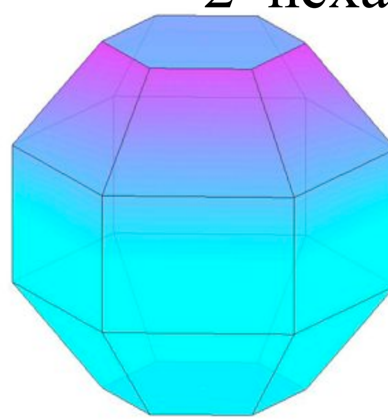

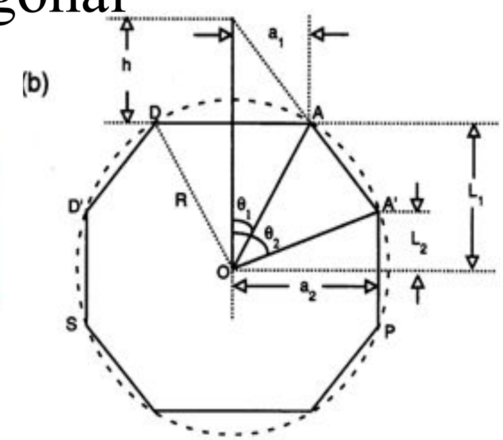

Ohtake (1970)

Field Campaign Information

Field Campaign	Location	Instruments	Number of PSDs
FIRE-1 (1986)	Madison, WI	2D-C, 2D-P	246
FIRE-II (1991)	Coffeyville, KS	Replicator	22
ARM-IOP (2000)	Lamont, OK	2D-C, 2D-P, CPI	390
TRMM KWAJEX (1999)	Kwajalein, Marshall Islands	2D-C, HVPS, CPI	418
CRYSTAL-FACE (2002)	Off coast of Nicaragua	2D-C, VIPS	41

Probe size ranges are: 2D-C, 40-1000 μm; 2D-P, 200-6400 μm; HVPS (High Volume Precipitation Spectrometer), 200–6100 μm; CPI (Cloud Particle Imager), 20-2000 μm; Replicator, 10-800 μm; VIPS (Video Ice Particle Sampler): 20-200 μm.

Ice Cloud Microphysical Model (Baum et al., 2005a)

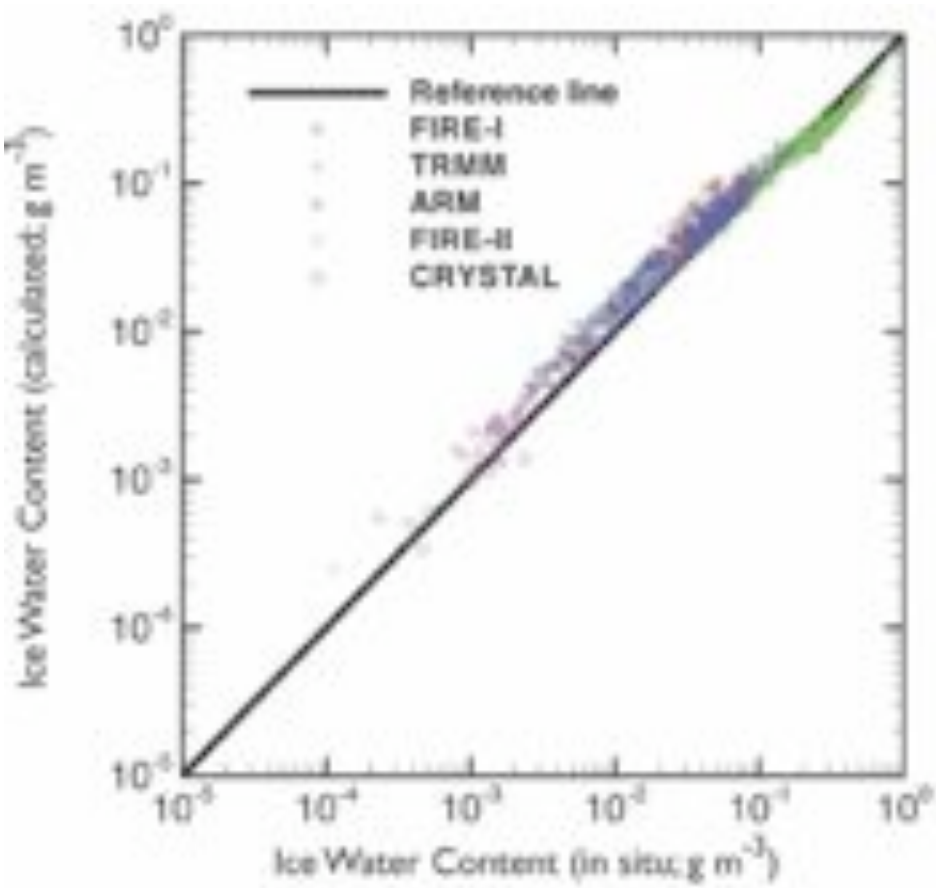

- Particle's maximum dimension D < 60 μm

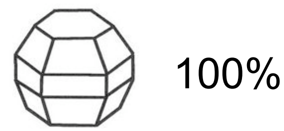

- 60 μm < *D* < 1000 μm

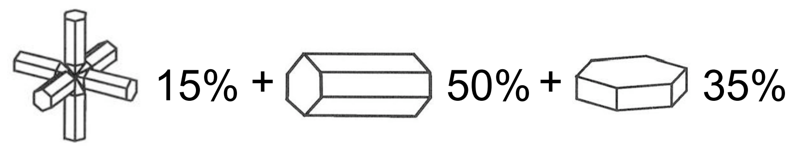

- 1000 μm < D < 2500 μm

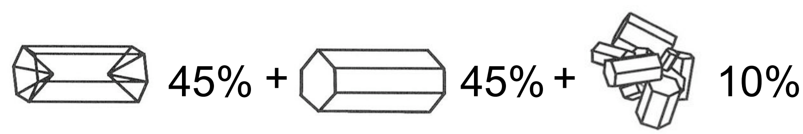

- 2500 μm < D

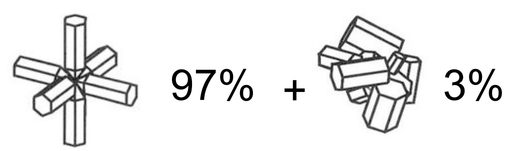

$$IWC = \rho_i \int_{D_{min}}^{D_{max}} \left[\sum_{i=1}^{N} f_i(D) V_i(D) \right] N(D) \mathrm{d}D$$

Mixing schemes for ice cloud particles
(Baum et al. 2005a)

Three-year Climatology of Ice Cloud Radiative Forcing

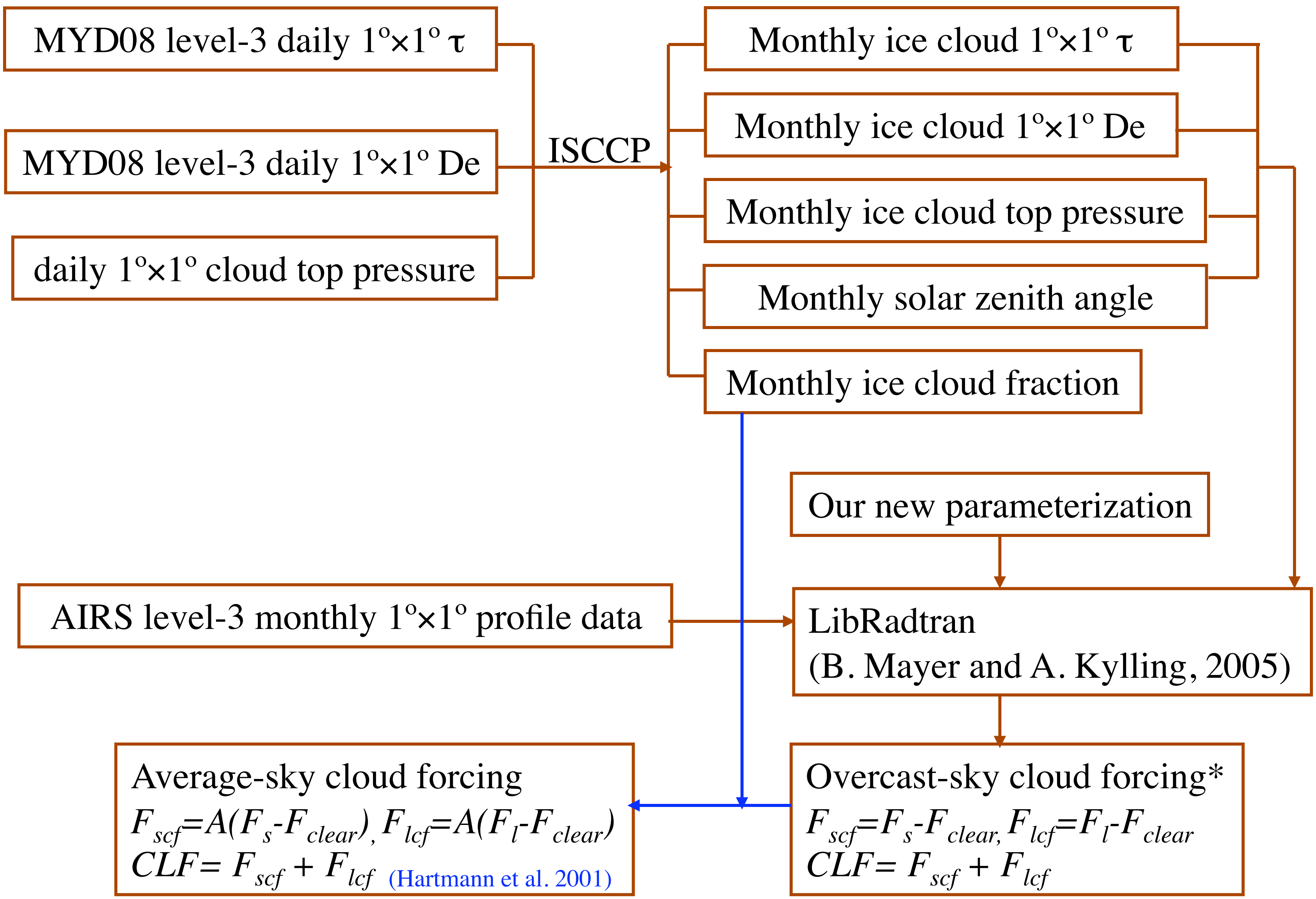

Ice cloud Radiative Forcing: MODIS Collection 004 vs 005

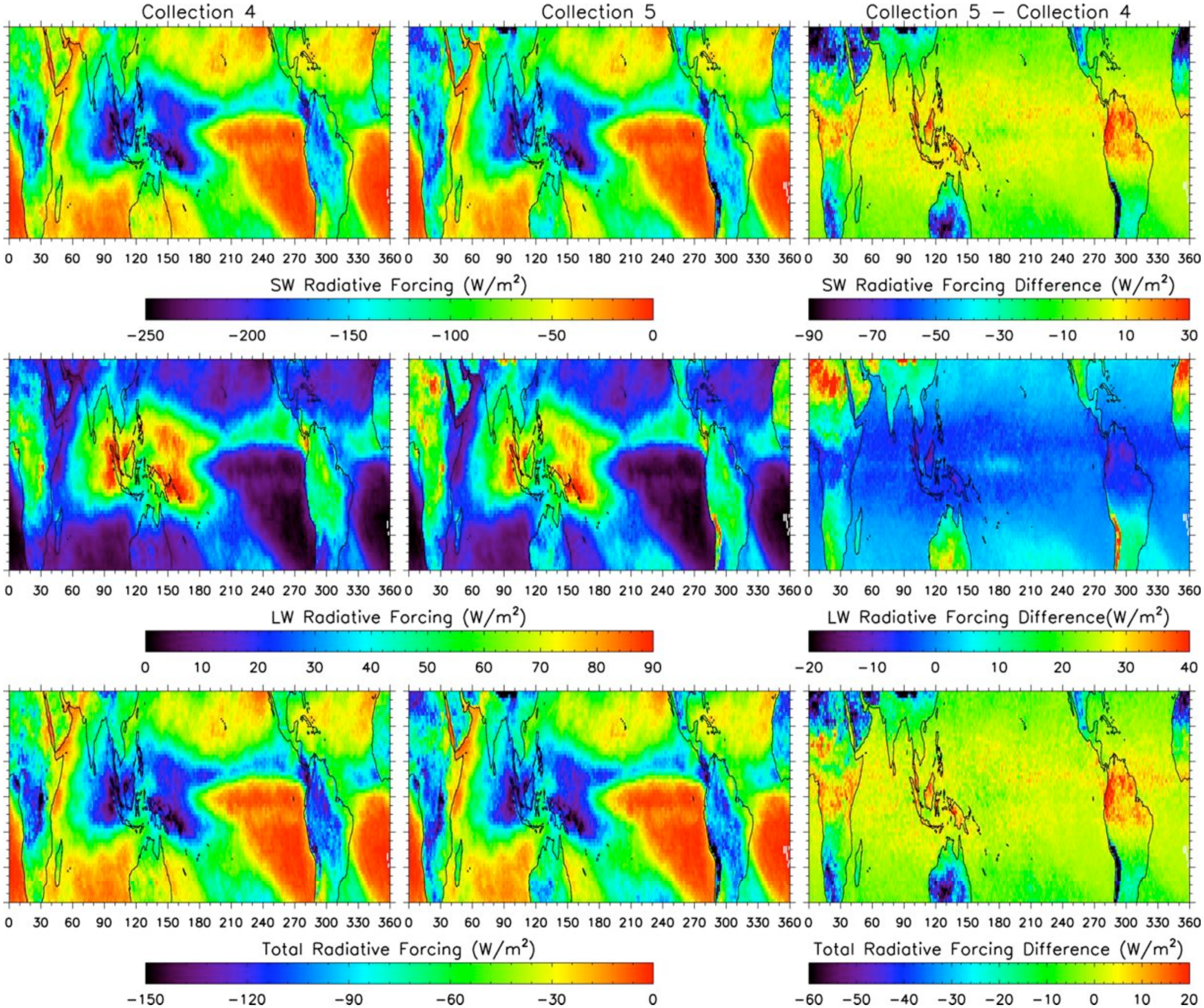

Solar zenith angle θ_0 = 60º, Duration of sunlight is assumed to be 12 hours, Tropical standard atmospheric profile

Improvements to Scattering models

- New treatment of ray-spreading results in the removal of the term relating to delta-transmission energy at the forward scattering angle.

- Improved the mapping algorithm: the single-scattering properties from the new algorithm smoothly transition to those from the conventional geometric optics method at large size parameters.

- Semi-analytical method developed to improve the accuracy of the first-order scattering (diffraction and external reflection).

- Semi-empirical method is developed to incorporate the edge effect on the extinction efficiency and the above/below-edge effects on the absorption efficiency.

Progress toward complex particle shapes

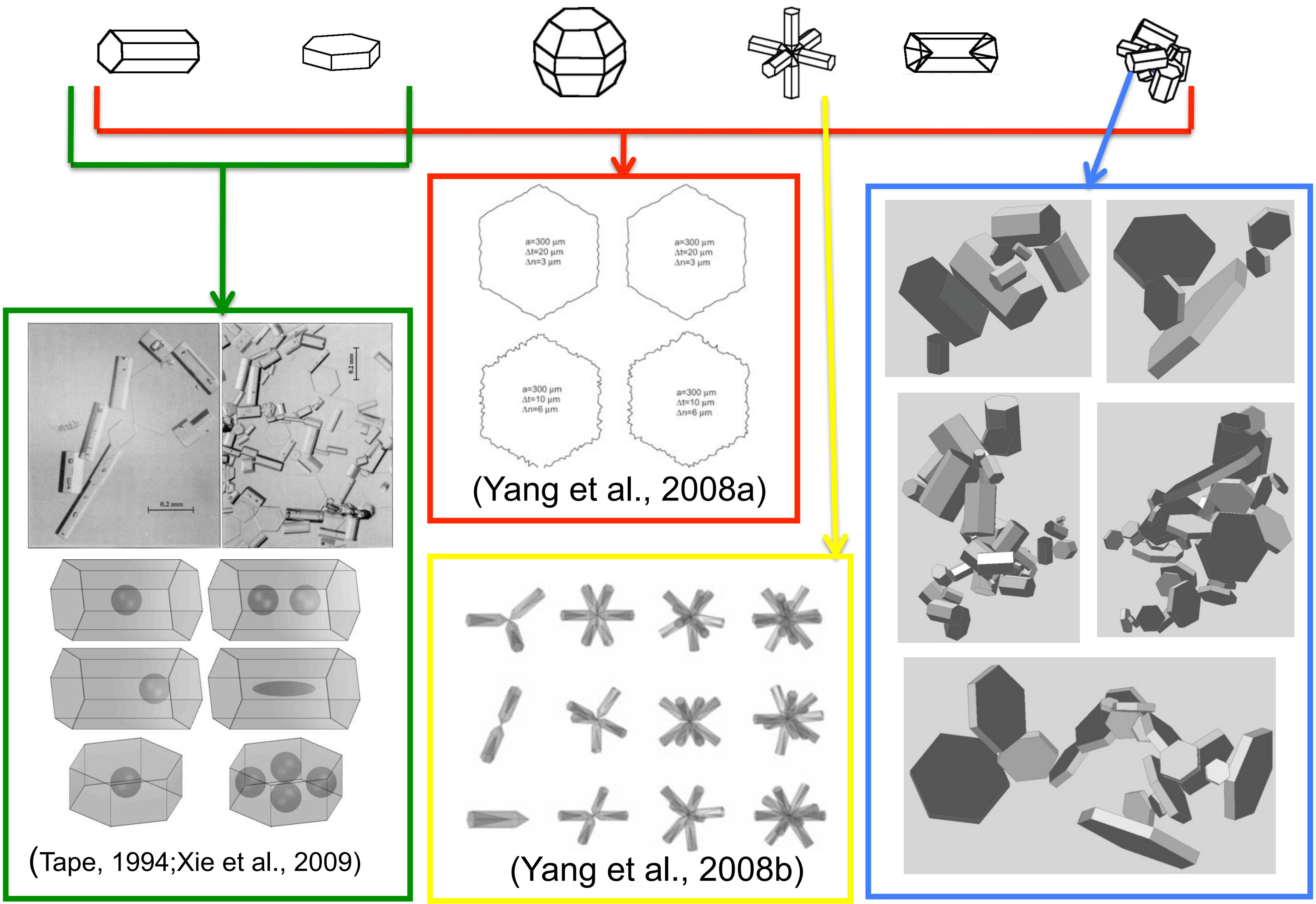

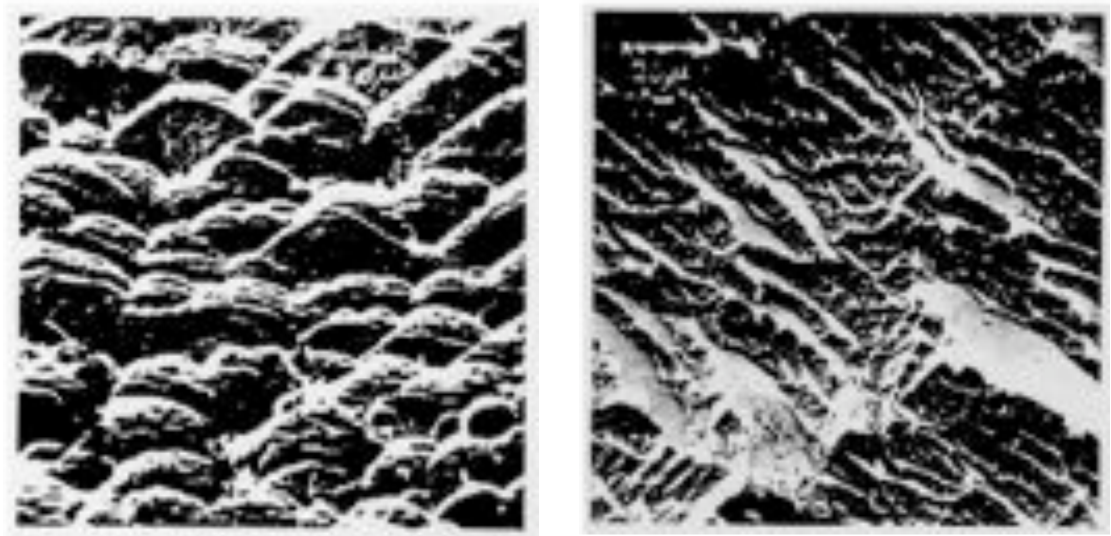

Surface roughness were observed for single crystals and polycrystalline ice by using an electronic microscope. Images adapted from Cross, 1968

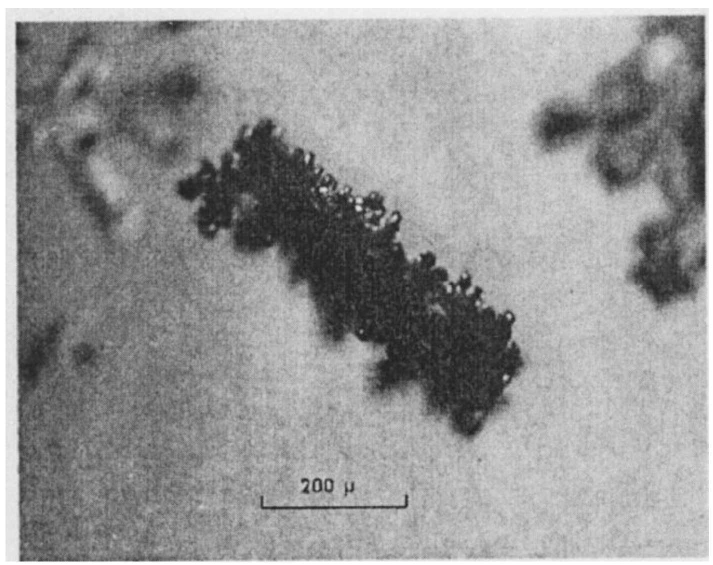

The image of a rimed column ice crystal (adapted from Ono, 1969). The surface roughness of this ice crystal is evident.

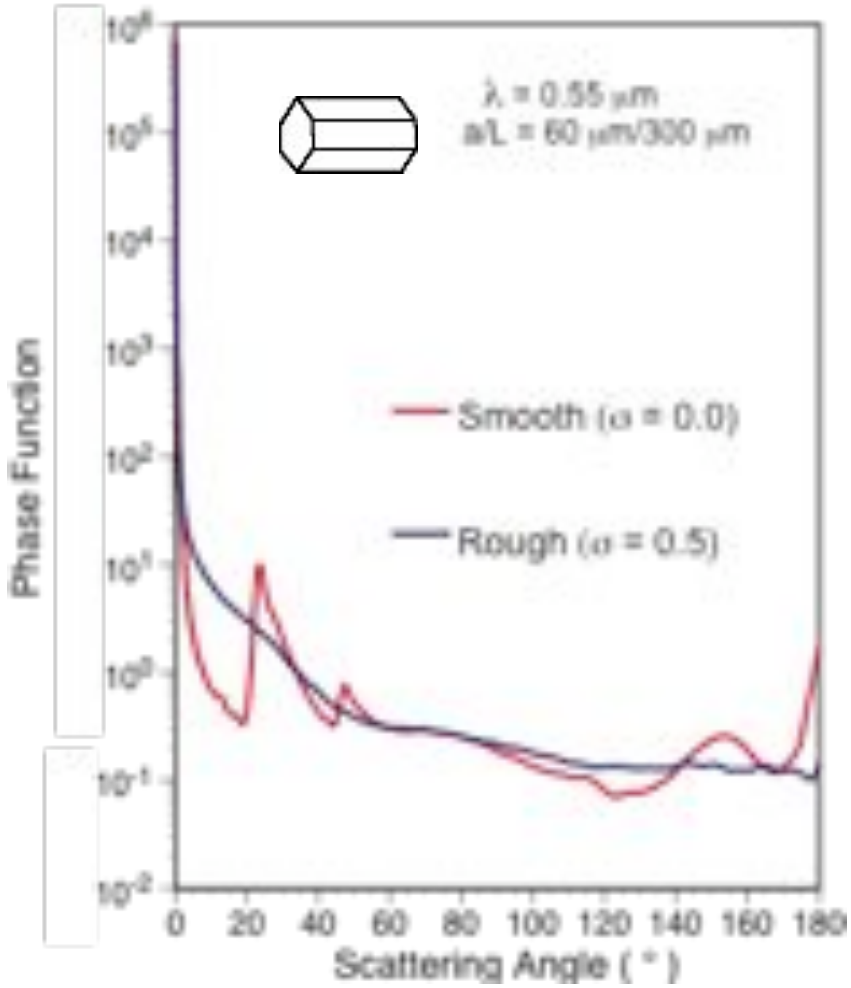

As articulated by Mishchenko et al. [1996] on the basis of the observations reported in the literature, halos are not often seen in the atmosphere and the phase functions associated with ice clouds might be featureless with no pronounced halo peaks. One of the mechanisms responsible for the featureless phase function might be the surface distortion or roughness of ice crystals

Effect of particle surface roughness on retrievals: Ice cloud optical thickness and effective particle size

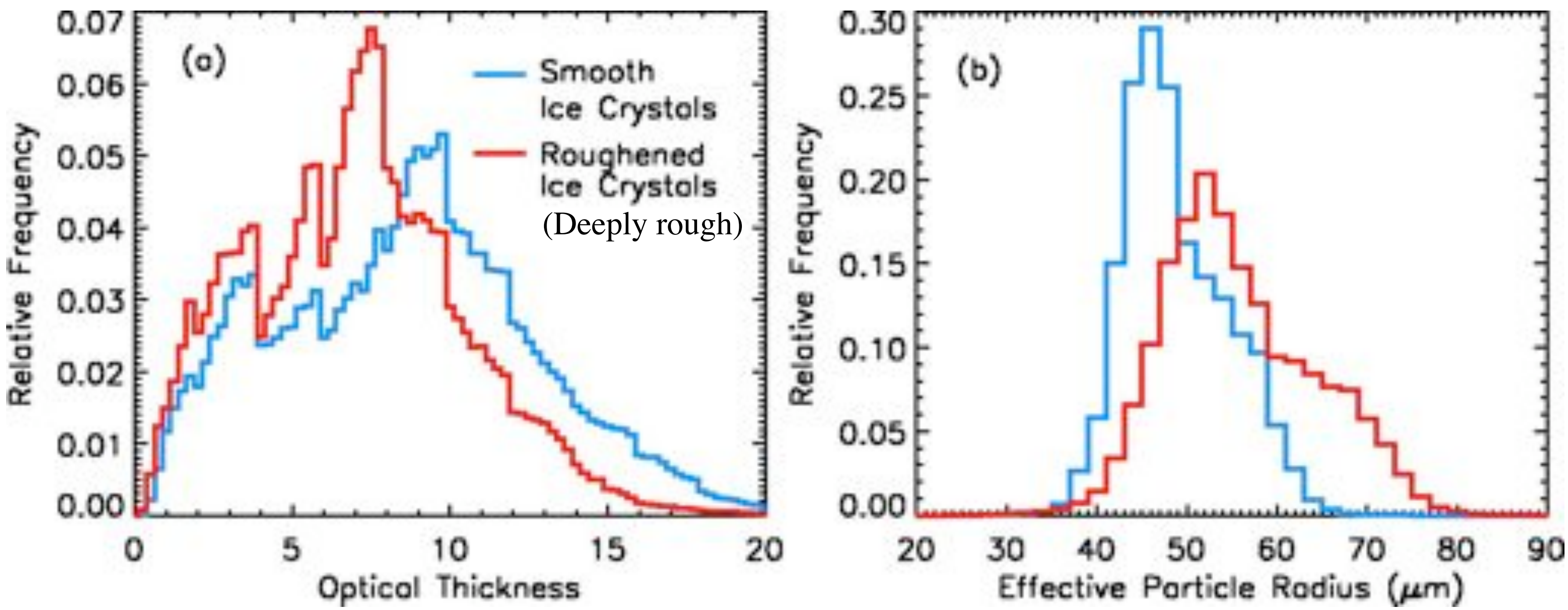

Differences between the MODIS and POLDER ice cloud models

Bulk scattering model

- MODIS: Baum05 model (Baum, Yang and co-authors, 2005)
- POLDER: IHM model (C.-Labonnote et al. 2000)

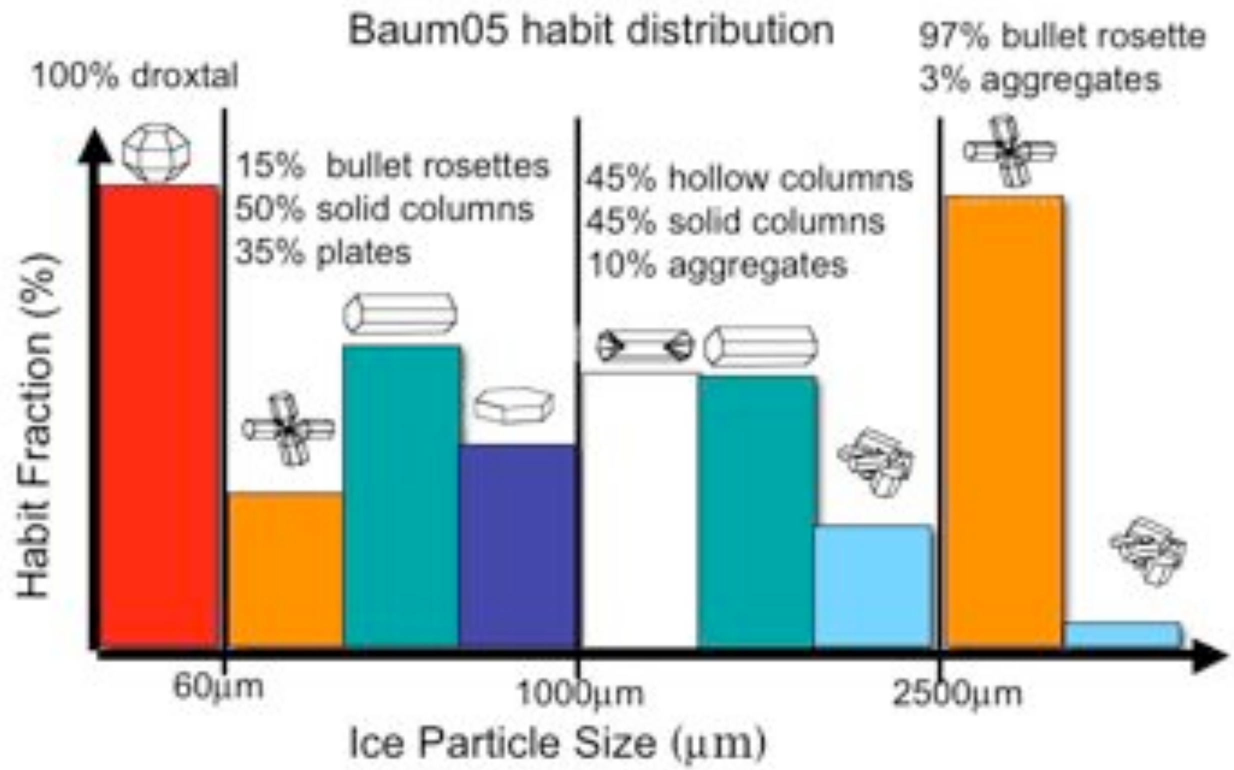

IHM model

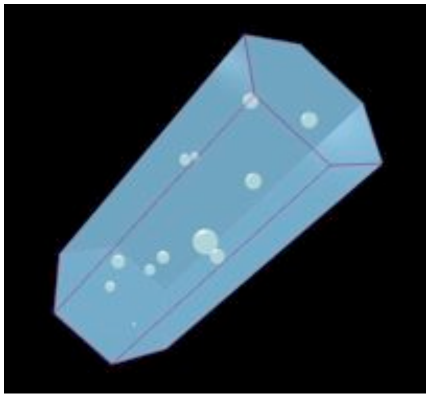

Courtesy of
Dr. Jerome Riedi

Comparison between MODIS and POLDER Retrievals
(Zhang, Yang and co-authors, 2009)

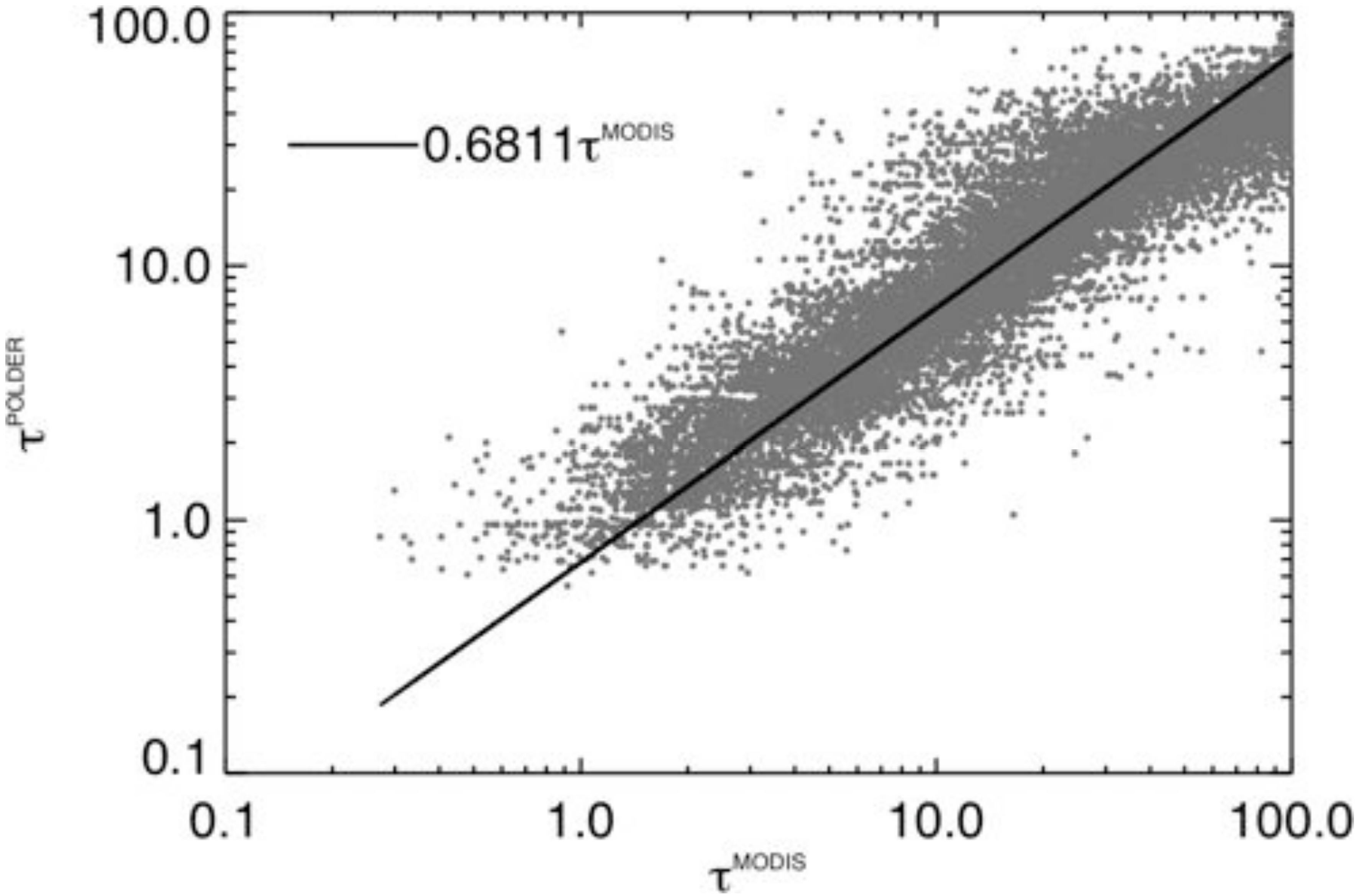

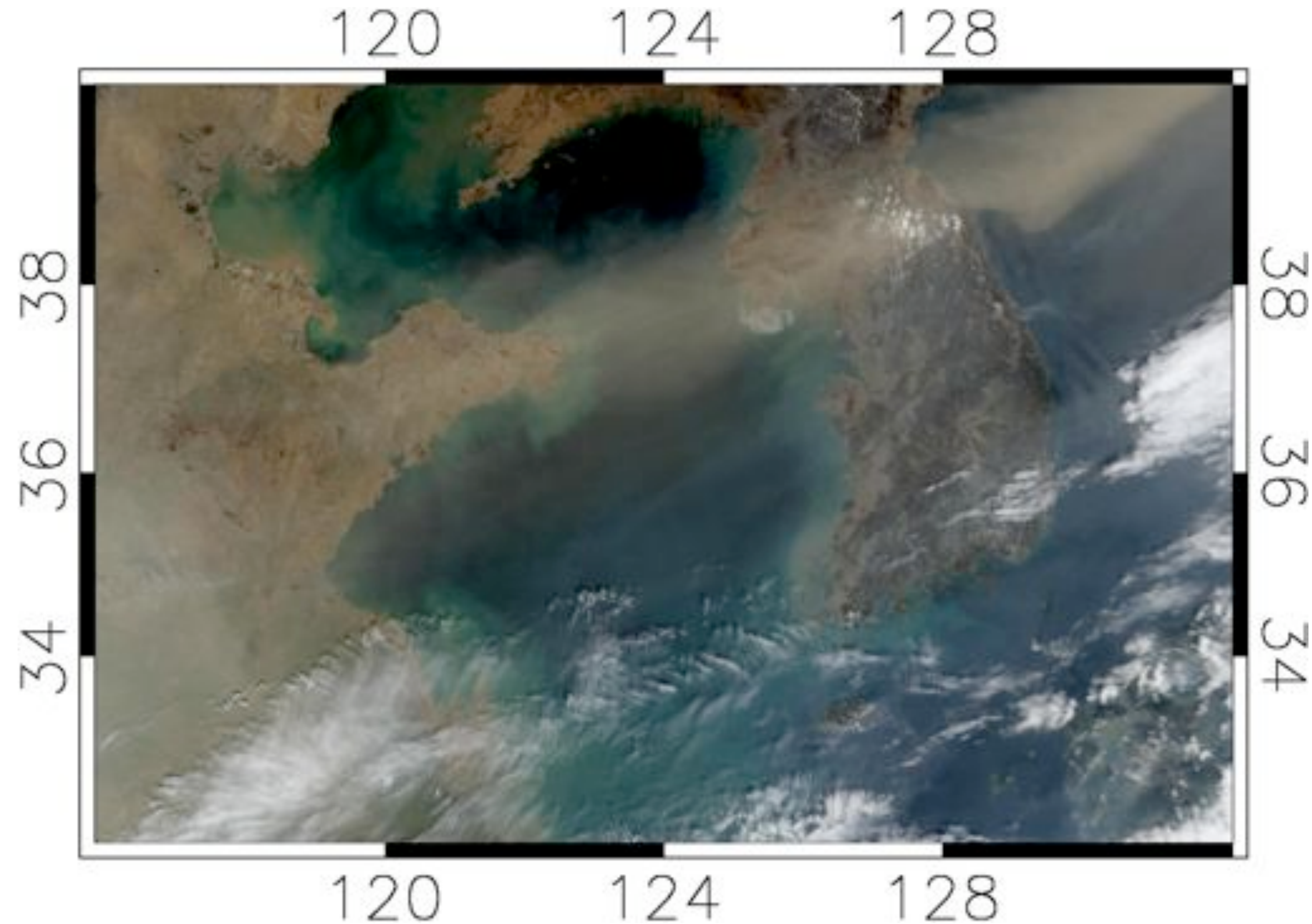

Asian Dust

MODIS RGB (0.65μm, 0.55μm, 0.47μm) Image

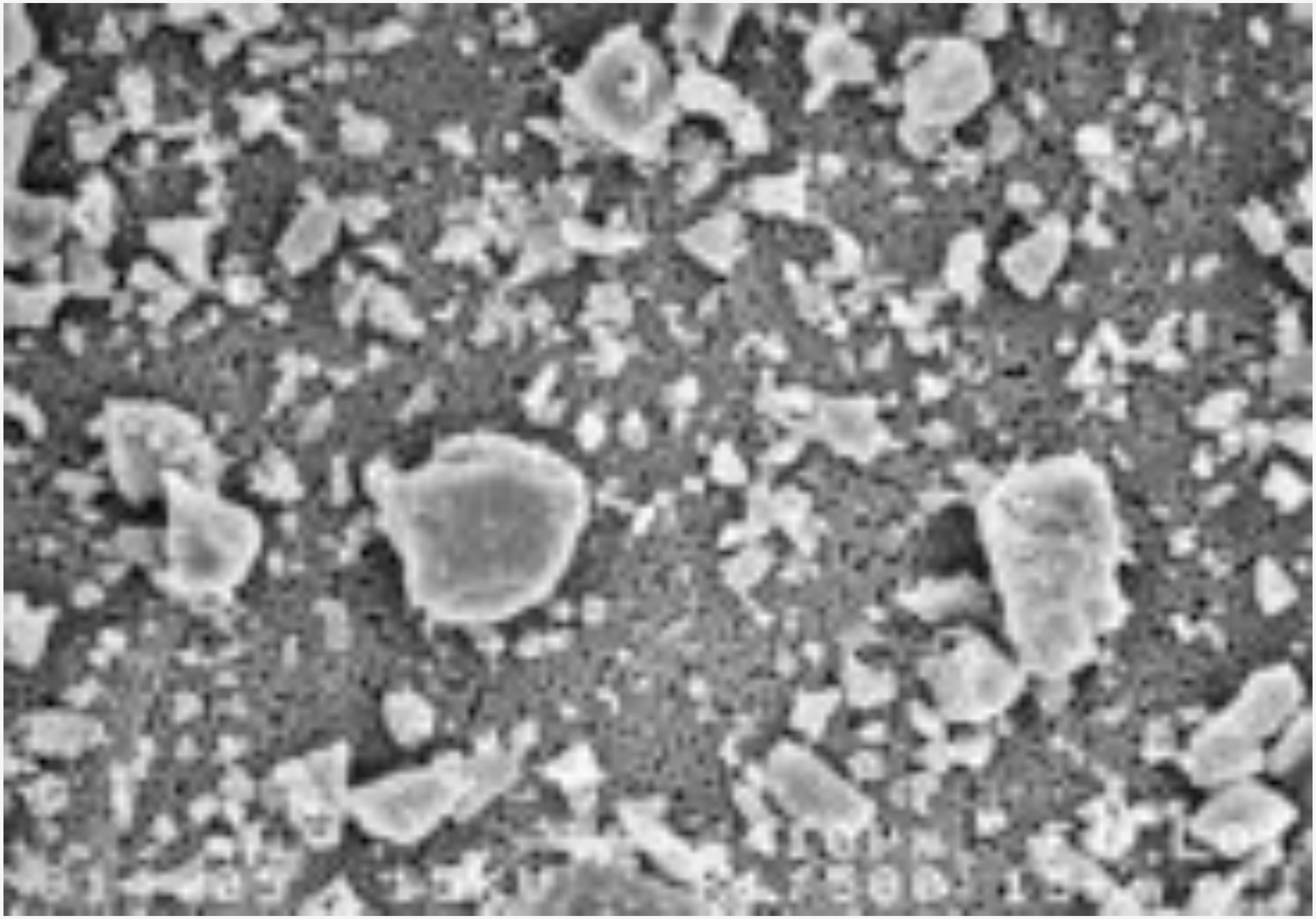

Mineral aerosols sample (feldspar) SEM image (Volten et al., 2001). Dust aerosols are exclusively irregular particles with arbitrary geometries.

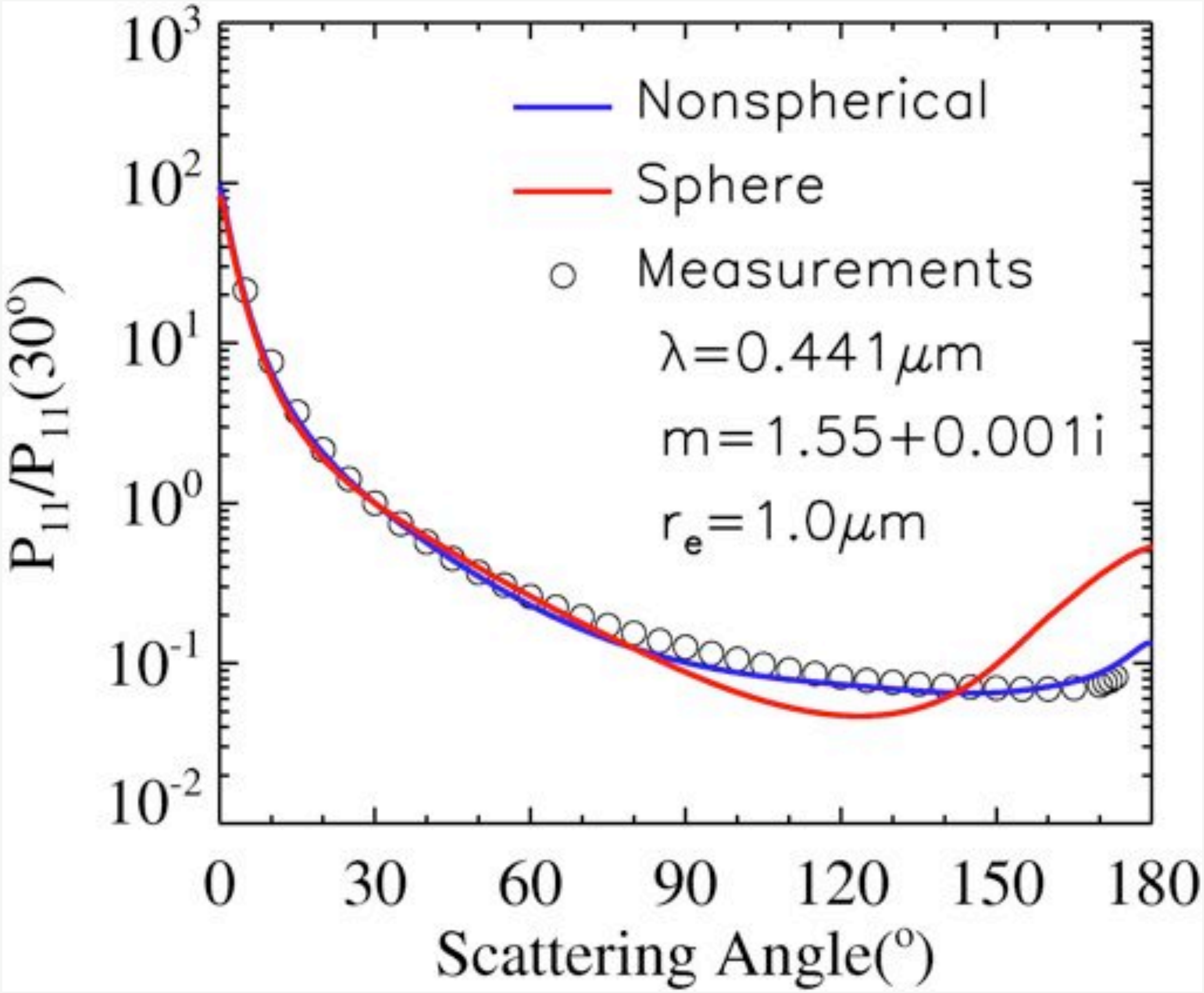

Comparison between the phase functions computed for spherical and nonspherical dust particles (Feng, Yang, Kattawar and co-authors, 2009). The symbols indicate laboratory measurements (Volten et al. 2001).

Simulated solar reflectance at the top of a dusty atmosphere. Spherical and nonspherical shapes are assumed for dust particles (Yang et al. , 2007).

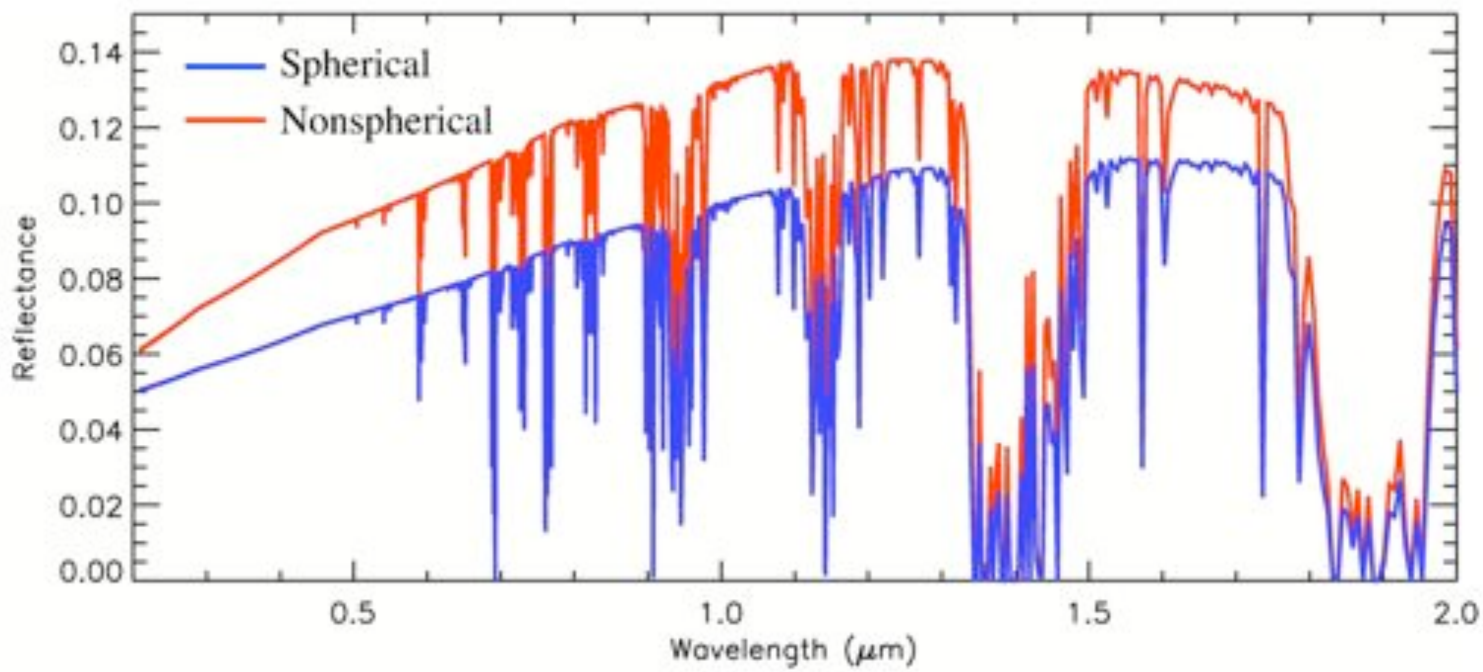

- These results indicate that the equivalent sphere approximation leads to an underestimate of the albedo of a dusty atmosphere. This underestimate has an important implication to the study of the effect of airborne dust on the radiation budget within the atmosphere.

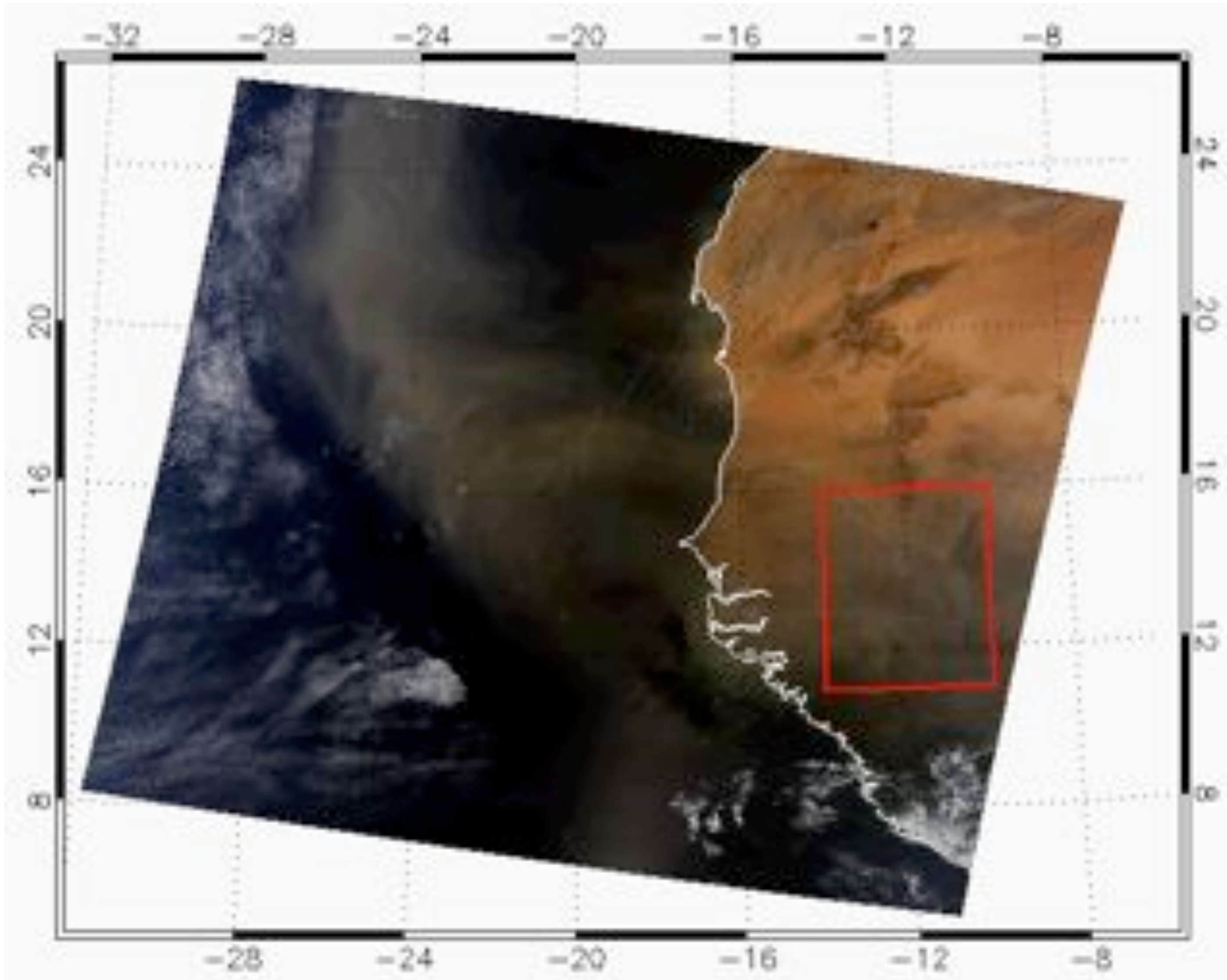

MODIS RGB image on March 2, 2003, showing a dust plume over West Africa. The area indicated by the small red box is used to retrieve dust AOD in the present sensitivity study (Feng, Yang, Kattawar, Hsu, Tsay and Laszlo, 2009).

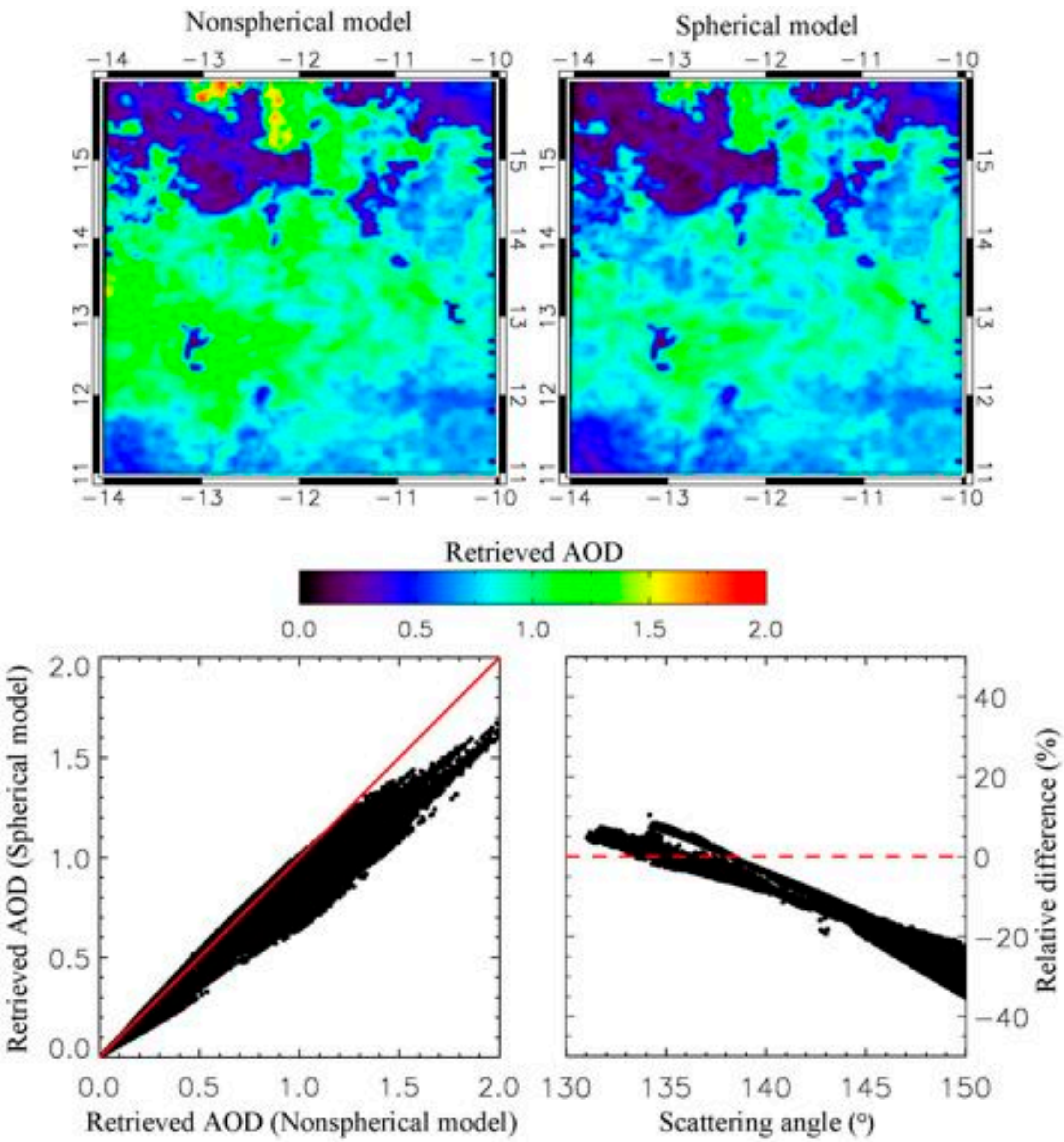

Upper panels: the retrieved dust AOD based on the nonspherical and sphere models.

Lower left panel: retrieved dust AOD based on the sphere model versus those based on the nonspherical model.

Lower right panel: the relative differences of the retrieved AOD (Feng, Yang, Kattawar, Hsu, Tsay and Laszlo, 2009).

Modeling Optical Properties of Mineral Aerosol Particles by Using Non-symmetric Hexahedra

(Bi, Yang, Kattawar and Kahn, 2010).

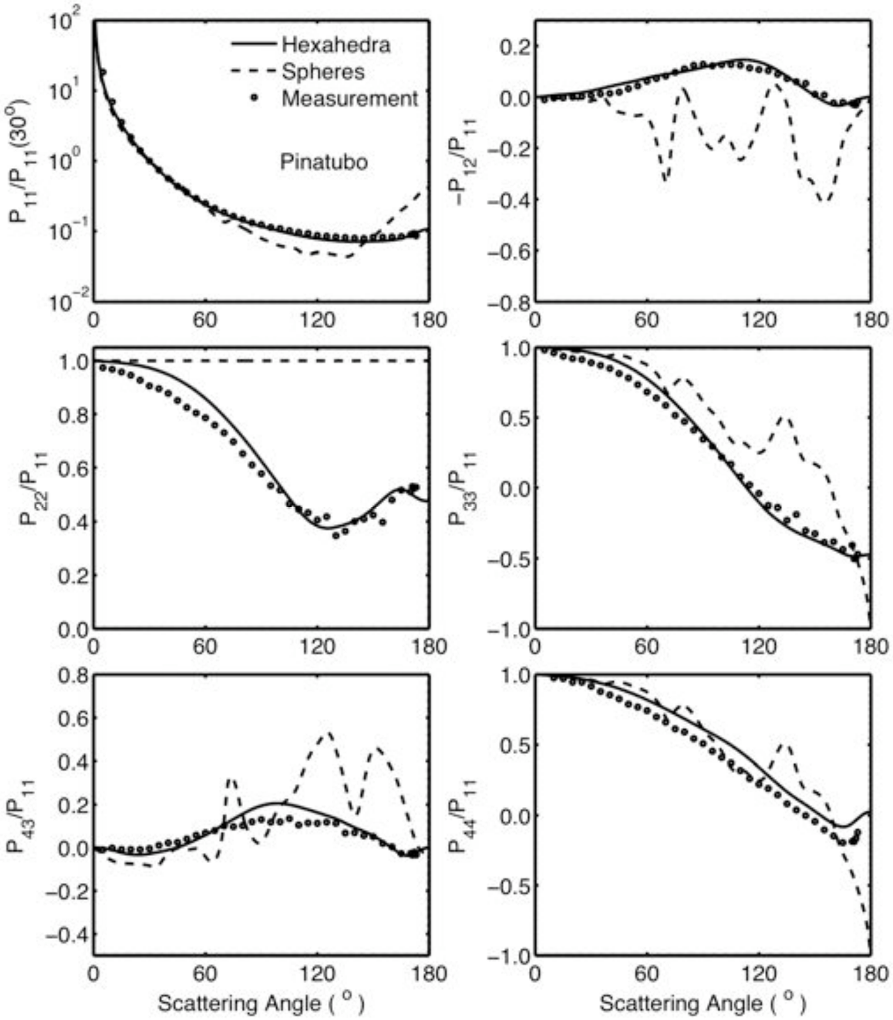

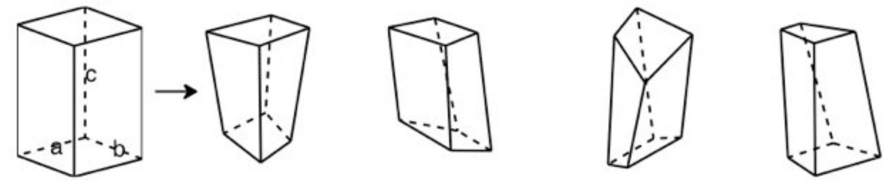

- Comparison of simulated results of hexahedra with measurements for Pinatubo aerosol particles at a wavelength of 0.633 μm.

Dust Aerosols: Observation & Modeling

- The CAM3+DEAD model is compiled on Linux platform and is run for ten years; DEAD is a dust entrainment and deposition module developed by Dr. Charlie Zender;
- The model horizontal resolution is T42, which is about 2.8 × 2.8 degrees; a slab ocean model is used. The vegetation in the model is updated with the result of BIOME3 model to better represent dust sources;
- Monthly model output of dust related variables were obtained to compare with former results;
- Multiple satellite AOD data sets are used to compare with the modeling results.

Model simulated dust mobilization and deposition

Dust mobilization

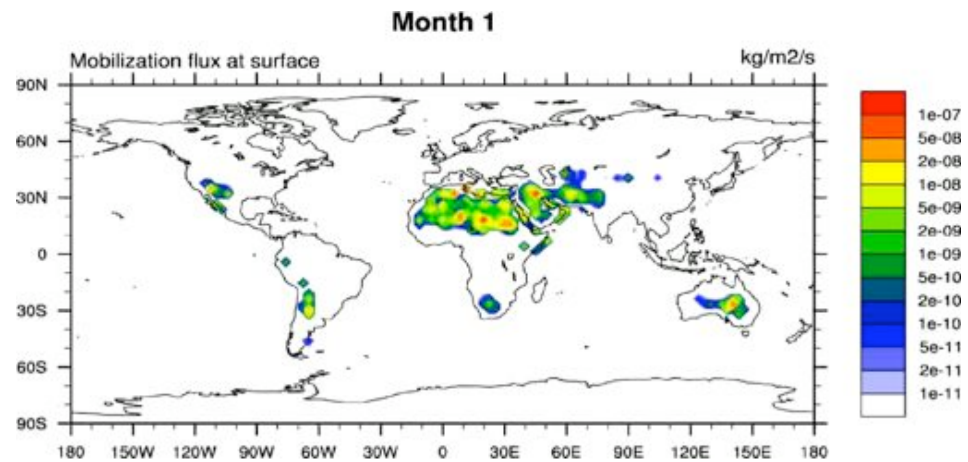

Dry deposition of dust

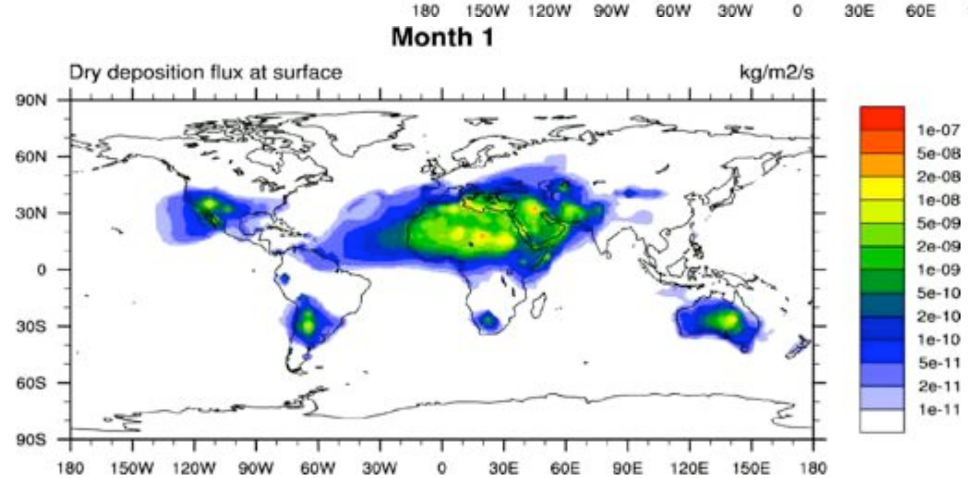

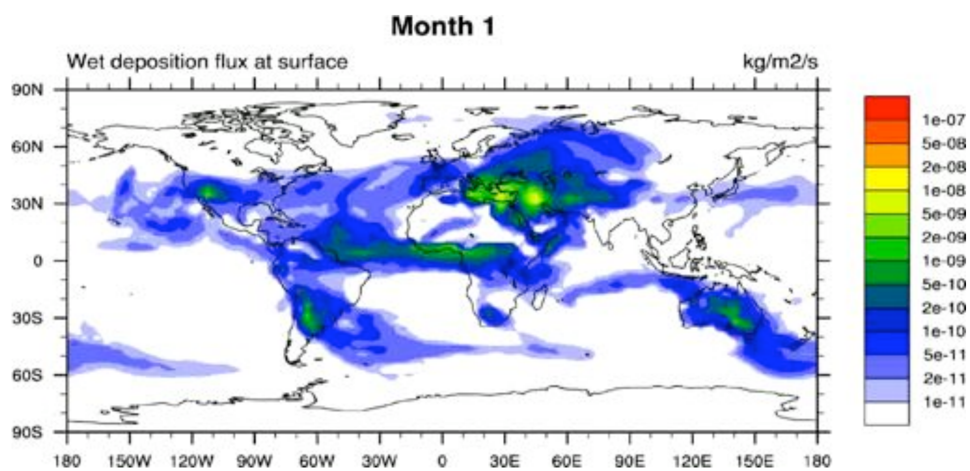

Wet deposition of dust

Modeled and Observed AOD - Spring

Dust optical depth

Dust optical thickness at 495nm

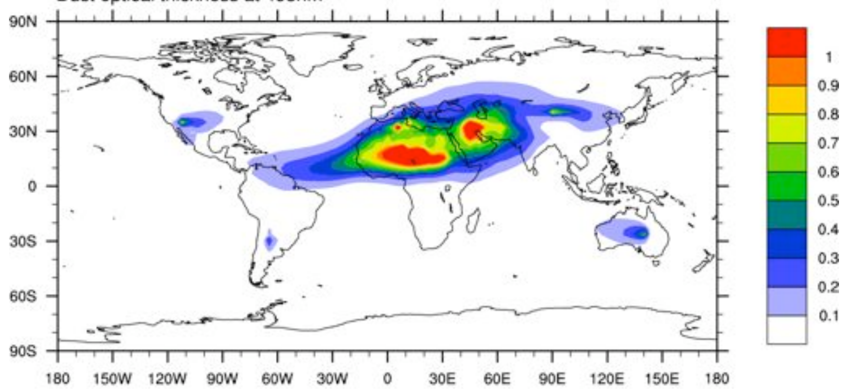

Global average is 0.0523481

MISR AOD climate average for SPR

Optical_depth_average

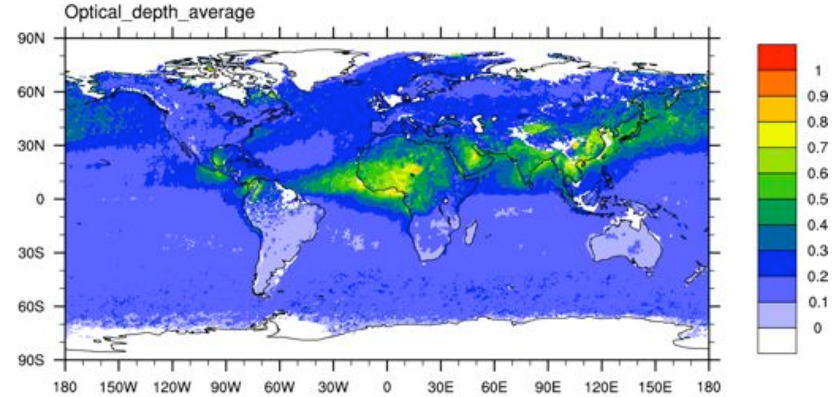

Global average is 0.212635

MODIS TERRA AOD 10 yr average climatology for SPR

Optical_Depth_Land_And_Ocean_Mean_Mean

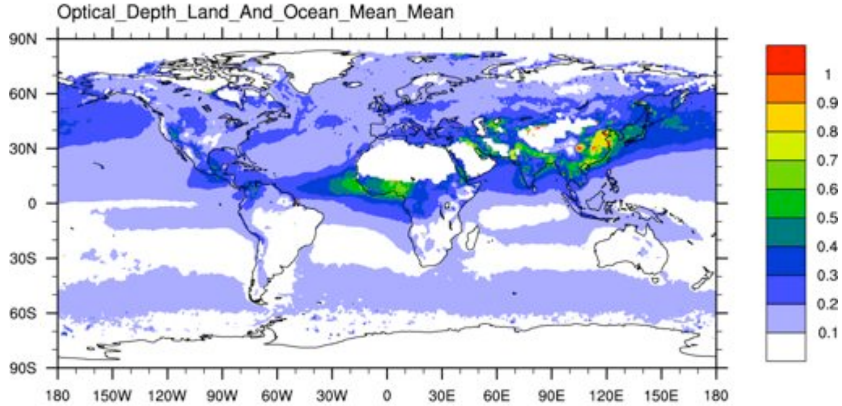

Global average is 0.162314

TOMS OMI averaged AI for Month 4

Aerosol_index

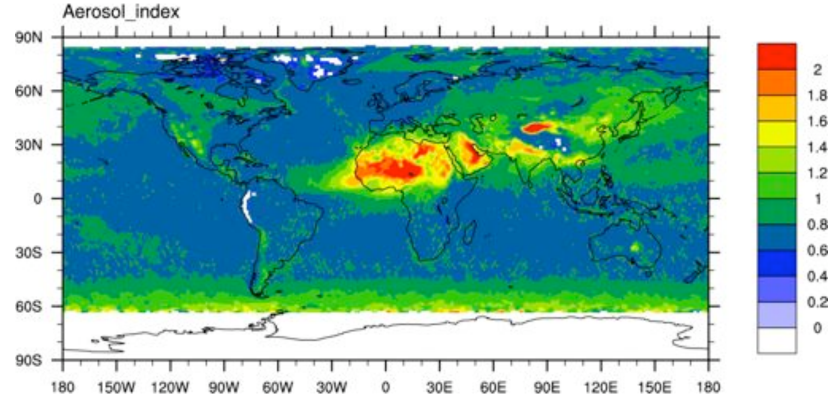

Modeled and Observed AOD - Fall

Dust optical depth

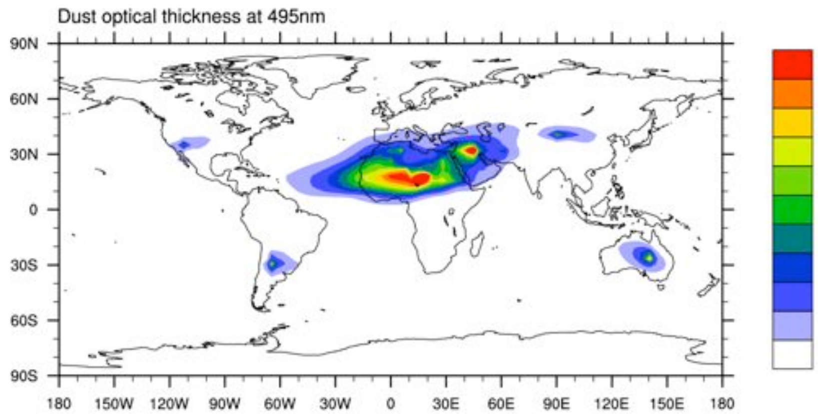

Global average is 0.0332353

MISR AOD climate average for FALL

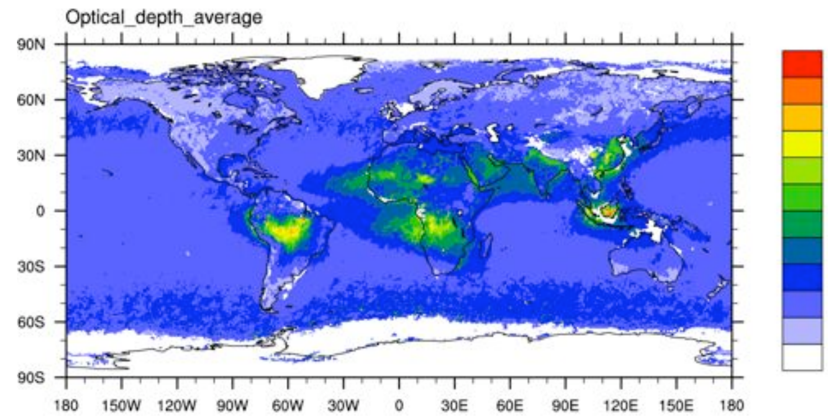

Global average is 0.192704

MODIS TERRA AOD 10 yr average climatology for FALL

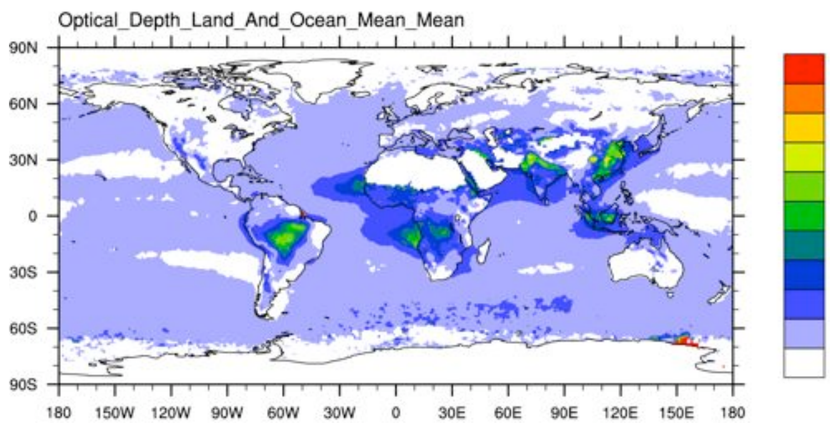

Global average is 0.149771

TOMS OMI averaged AI for Month 10

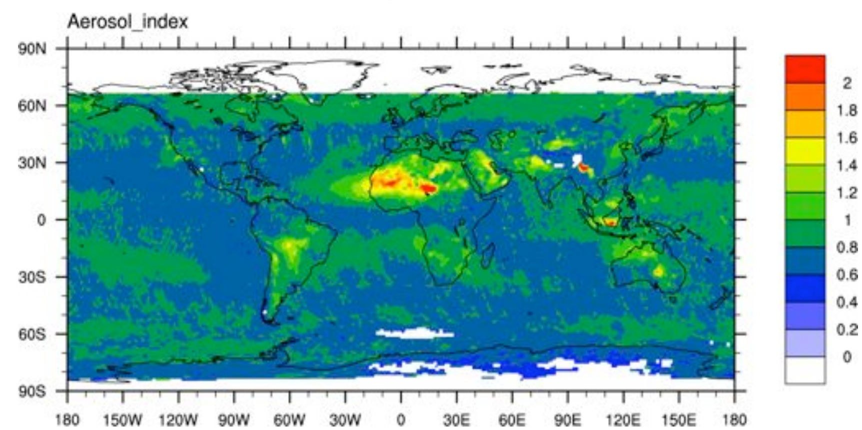

Modeled and Observed AOD – All year average

Dust optical depth

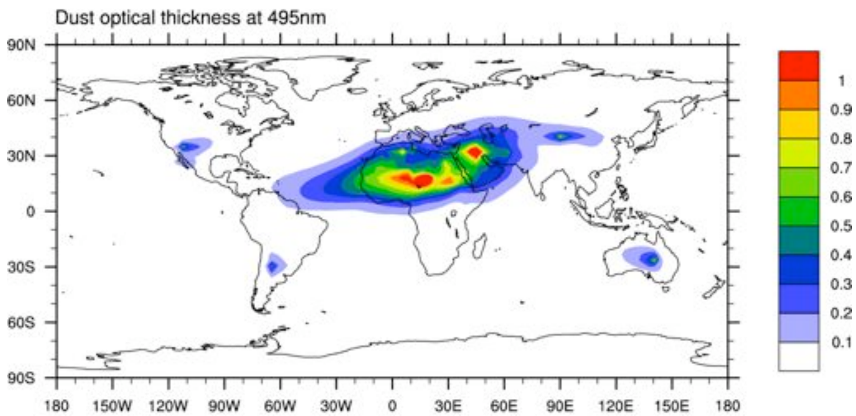

Global average is 0.0409387

MISR AOD average climatology: 2005-2008

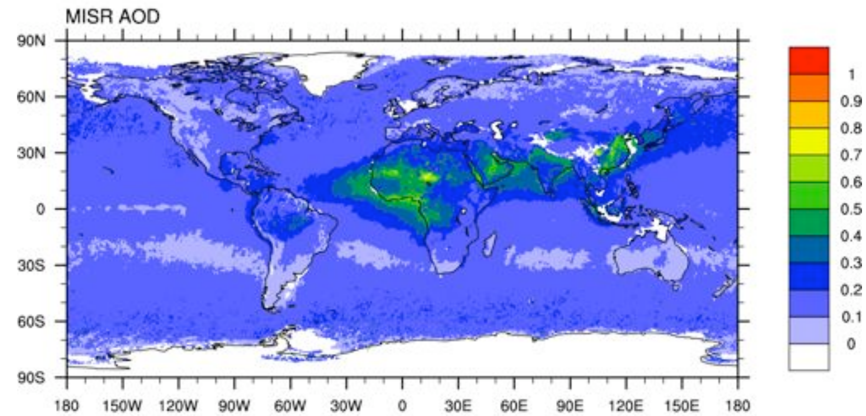

Global average is 0.162598

MODIS Aqua Combined AOD average climatology: 2005-2008

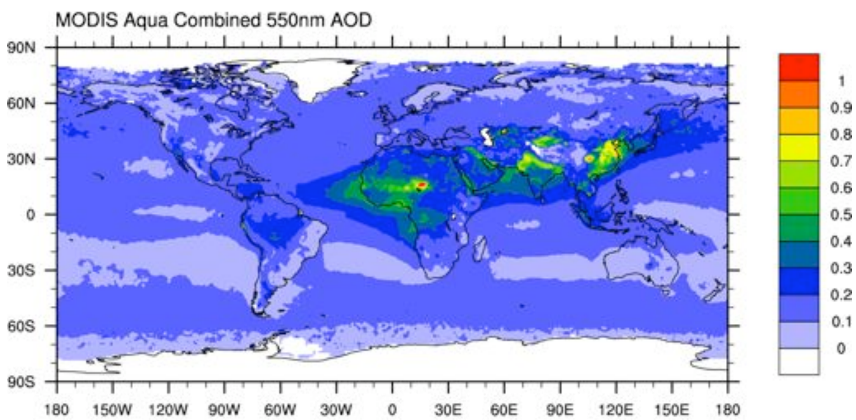

Global average is 0.146707

TOMS AI average climatology: 2005-2008

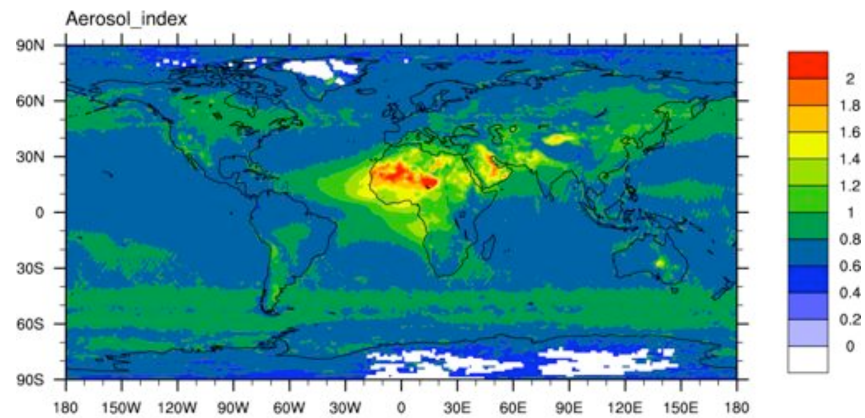

Global average is 0.78495

Dust radiative forcing

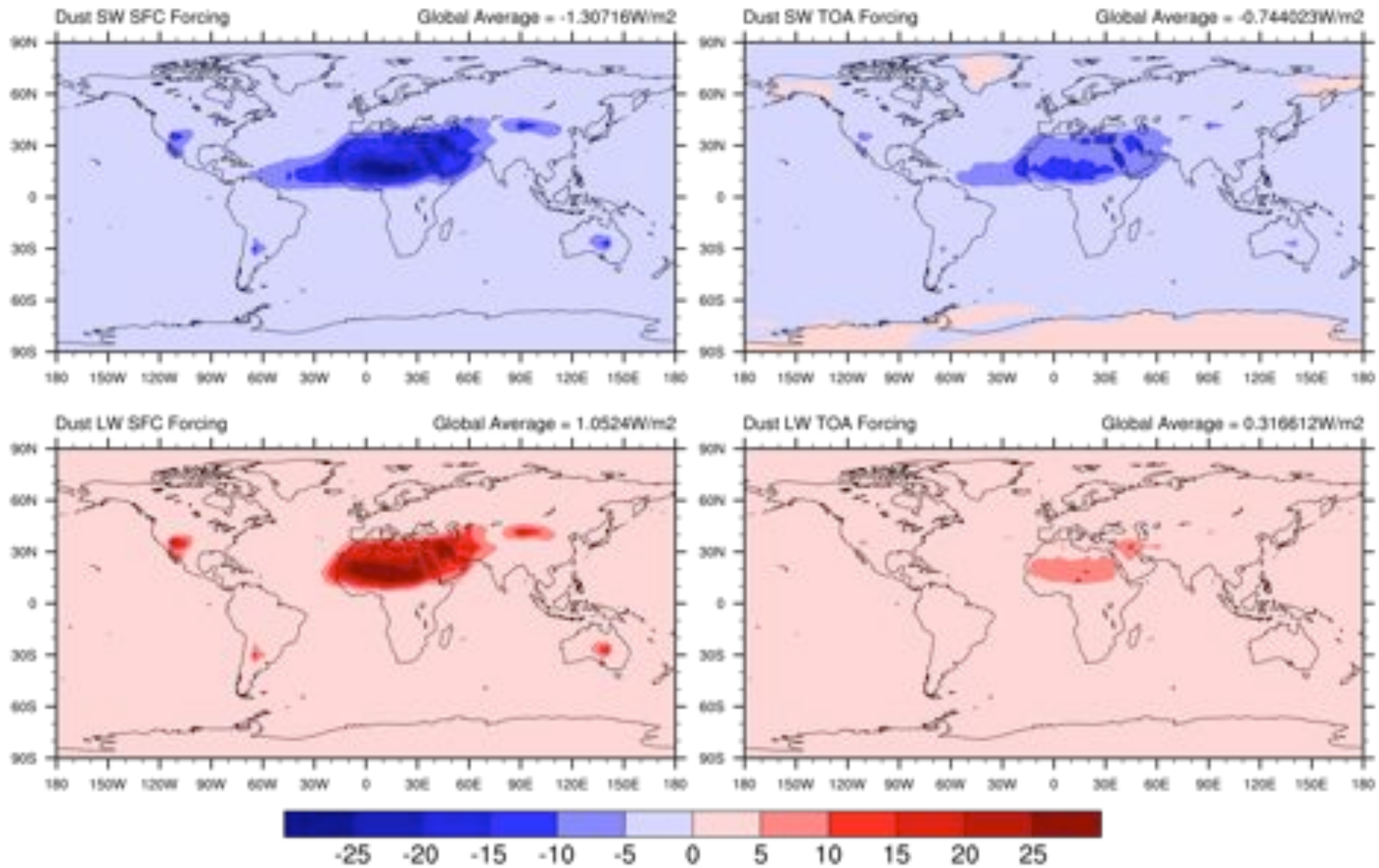

Fig. Simulated dust radiative effect: difference in Short-wave and Long-wave radiative flux at TOA and SFC in dust-on and dust-off cases

“Thin” Cirrus clouds

- “Thin” cirrus clouds are defined here as being those not detected by the operational MODIS cloud mask, corresponding to an optical depth value of approximately 0.3 or smaller, but are detectable in terms of the cirrus reflectance product based on the MODIS 1.375-µm channel;
- Our preliminary results show that thin cirrus clouds were present in more than 40% of the pixels flagged as “clear-sky” by the operational MODIS cloud mask algorithm;
- The present study shows positive and negative net forcings at the top of the atmosphere (TOA) and at the surface, respectively. The positive (negative) net forcing at TOA (the surface) is due to the dominance of longwave (shortwave) forcing. Both the TOA and surface forcings are in a range of 0-20 Wm^{-2}, depending on the optical depths of thin cirrus clouds.

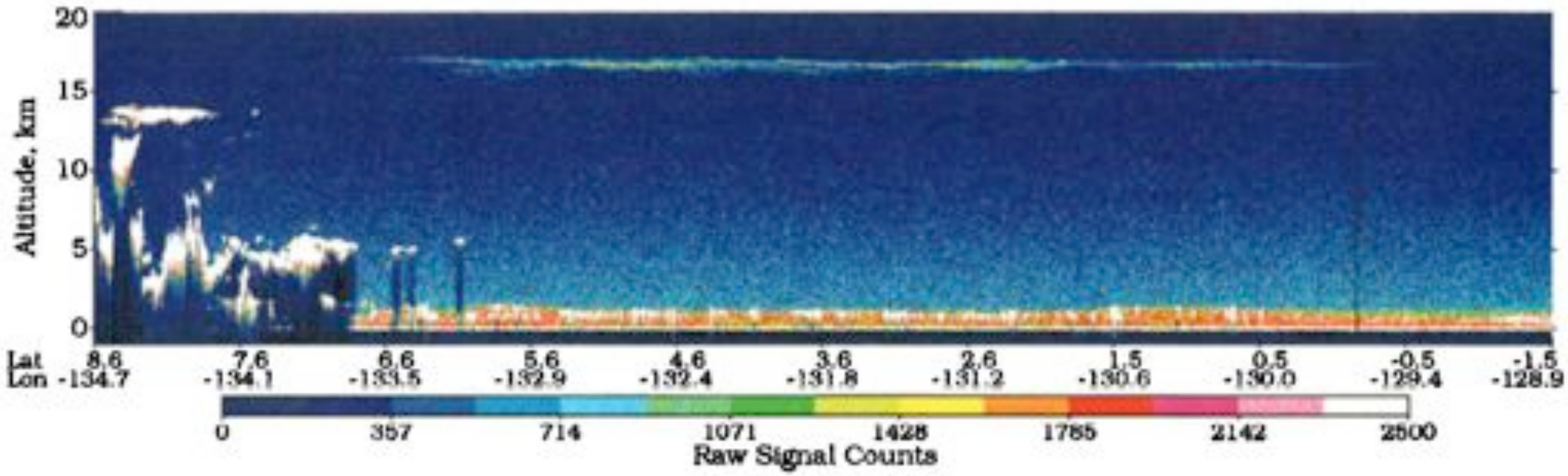

Cross-section of color-coded raw backscatter signal from the LITE 532 nm channel over the western Pacific Ocean. White indicates dense clouds or the ocean surface return, dark blue indicates clean atmosphere, reds and greens generally indicate aerosols. Laminar cirrus is seen at an altitude of 17 km. (Winker and Trepte, 1998).

Subvisible cirrus clouds

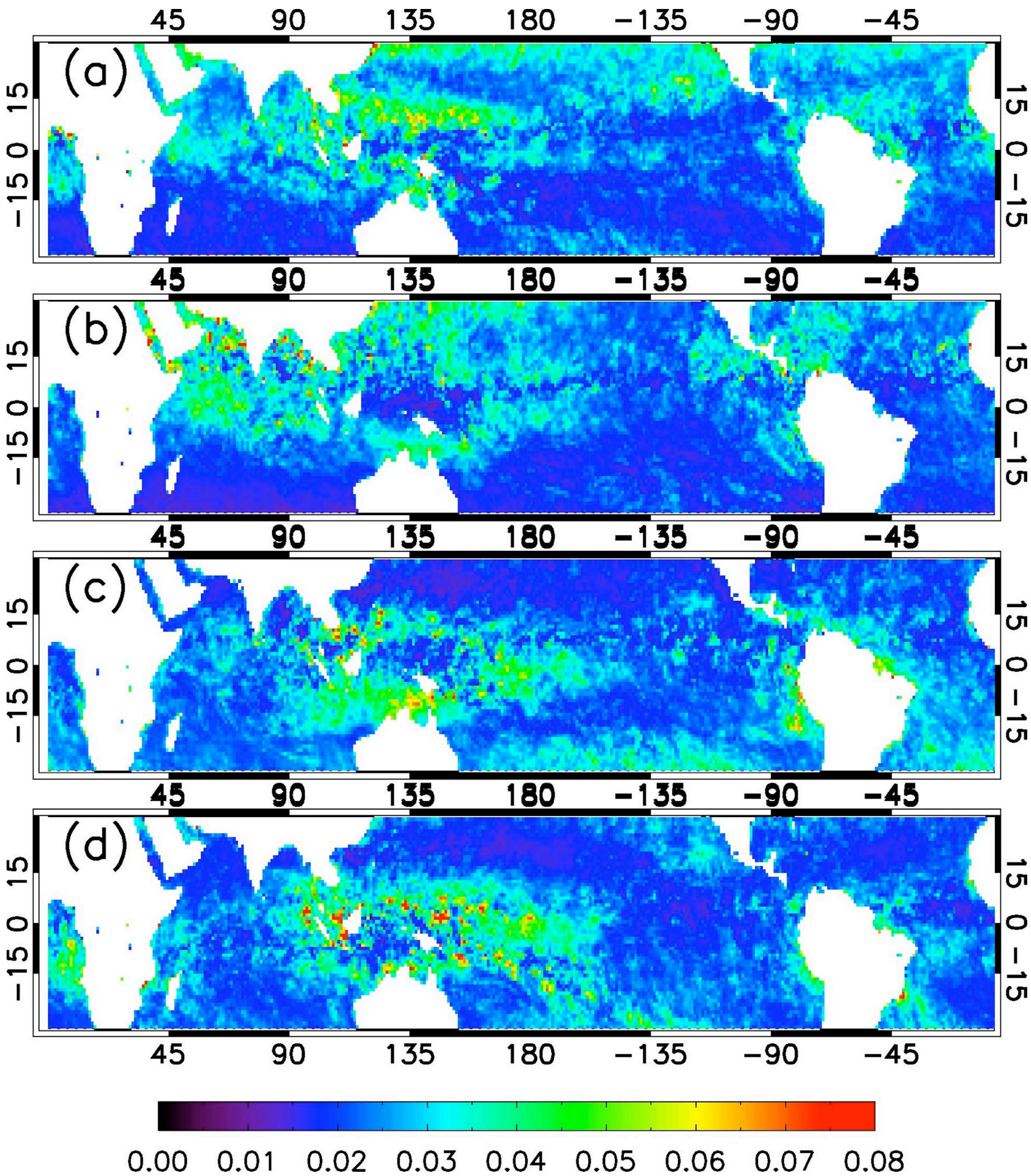

Optical depths of tropical thin cirrus clouds for the pixels flagged as "clear-sky" by MODIS for boreal (a) spring, (b) summer, (c) autumn, and (d) winter (Lee, Yang and co-authors, 2009)

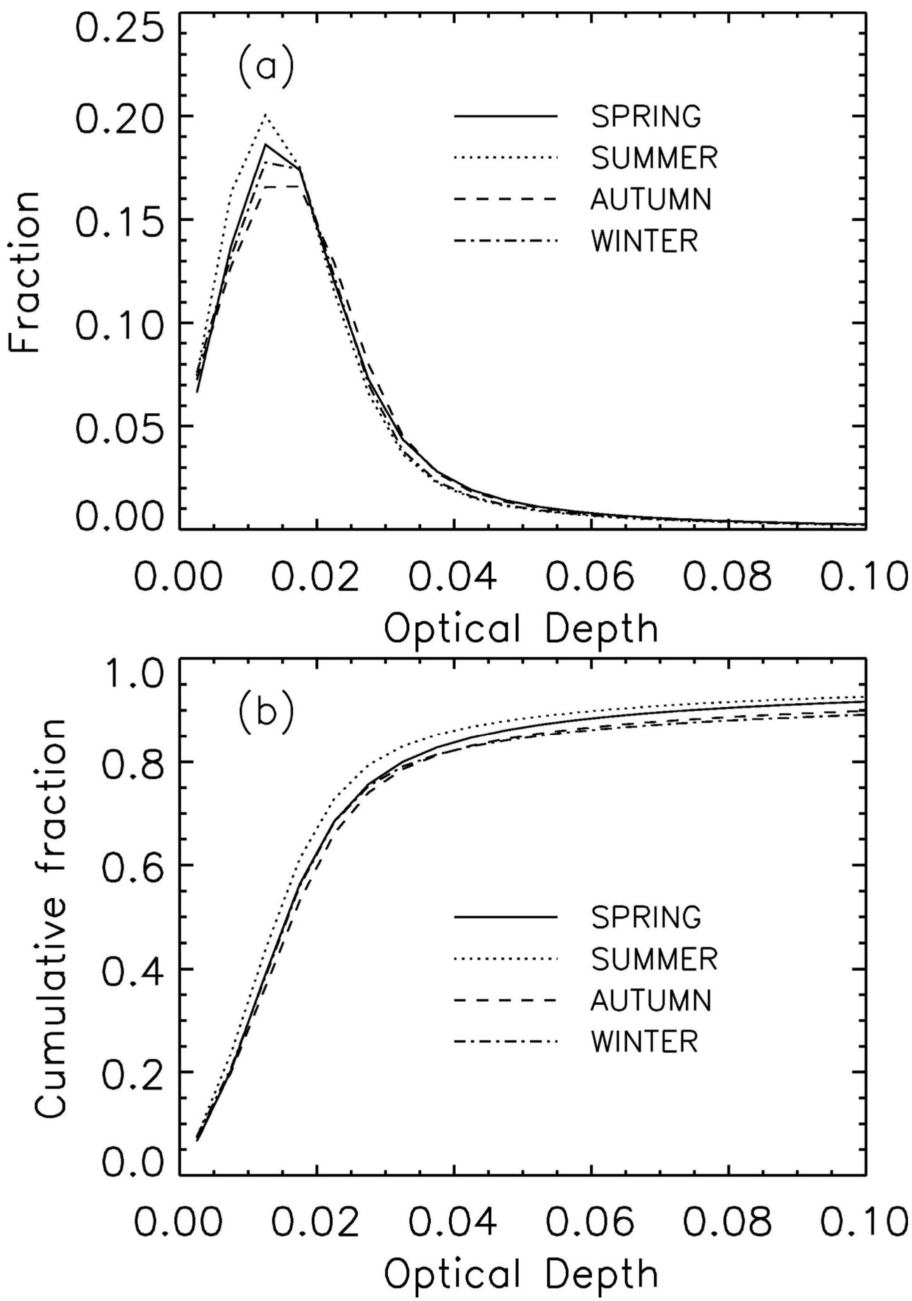

Subvisible cirrus clouds

(a) Histograms of optical depth of thin cirrus clouds retrieved between latitudes 30°S and 30°N for each of boreal seasons.

(b) Cumulative fractions of optical depth of thin cirrus clouds for each of boreal seasons.

Lee, Yang and co-authors (2009)

Radiative forcing of subvisible cirrus clouds

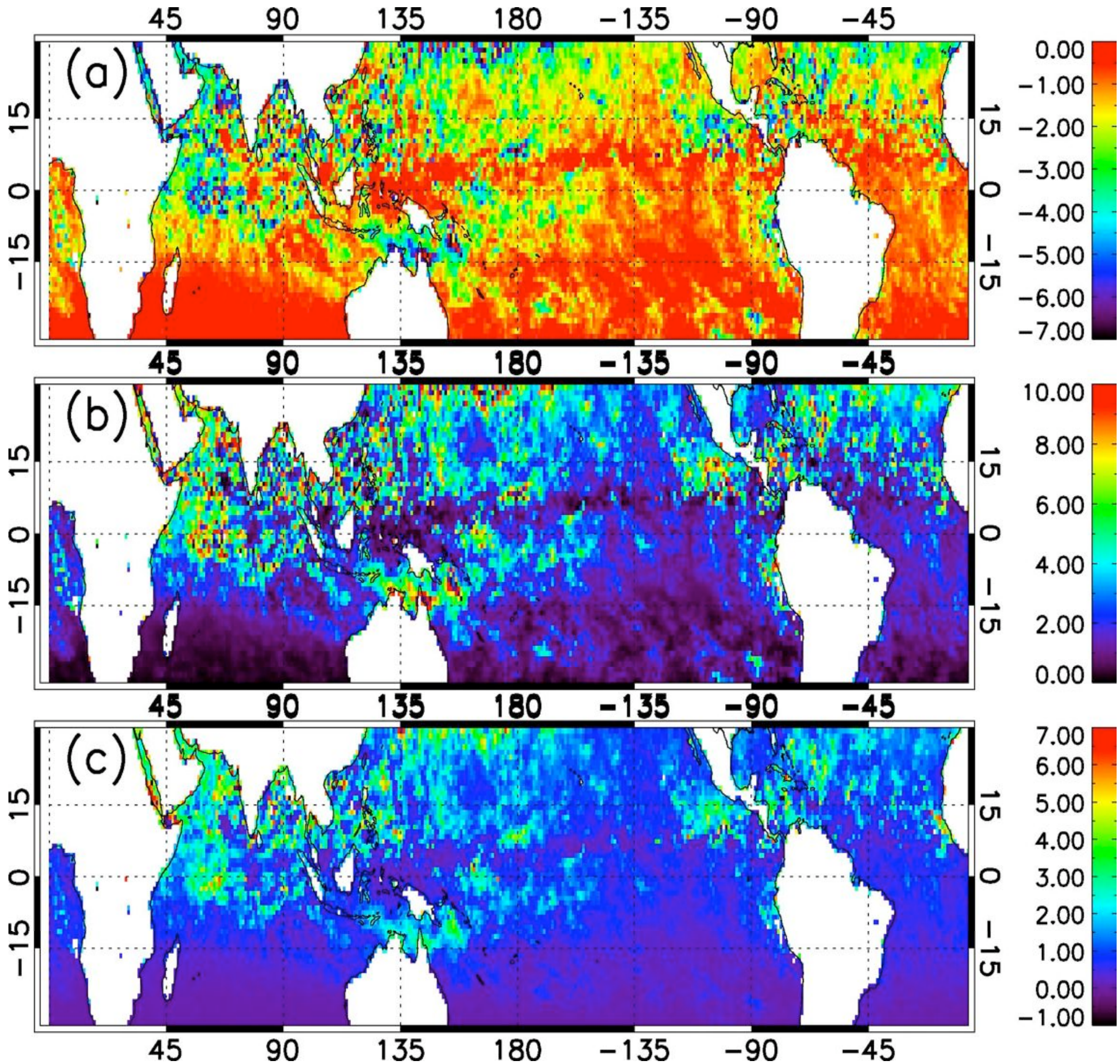

Spatial distributions of (a) shortwave, (b) longwave, and (c) net cloud radiative forcing at the top of the atmosphere for June 2005. Units are Wm^{-2} (Lee, Yang and coauthors, 2009)

Summary

- Research with MODIS cloud products:
  - comparisons of global properties with NCAR CAM3
  - comparisons of MODIS with POLDER and CALIPSO
  - collaboration with other groups working with MODIS data independently
- Use of MODIS cloud products to investigate tropical equatorial waves
- Improvements in deriving the single-scattering properties of aerosols and ice clouds:
  - new habits: hollow bullet rosettes, aggregates of plates
  - improved computational models
  - ice models being used by many EOS sensor teams
  - dust models include nonspherical particles
- We studied the distribution and radiative forcing of tropical "thin" cirrus clouds.